The Cryosphere Discuss., https://doi.org/10.5194/tc-2017-264
Manuscript under review for journal The Cryosphere
Discussion started: 8 December 2017

The Cryosphere Discussions
Open Access
EGU

Consumption of atmospheric methane by the Qinghai–Tibetan Plateau alpine steppe ecosystem

Hanbo Yun[1, 2, 3], Qingbai Wu[1*], Qianlai Zhuang[3*], Anping Chen[4]* Tong Yu[3], Zhou Lyu[3], Yuzhong Yang[1], Huijun Jin[1], Guojun Liu[1], Yang Qu[3], Licheng Liu[3]

1. State Key Laboratory of Frozen Soil Engineering, Northwest Institute of Eco–Environment and Resources, Chinese Academy of Sciences, Lanzhou, Gansu 730000, China

2. Key Laboratory for Land Surface Process and Climate Change in Cold and Arid Regions, Chinese Academy of Sciences, Lanzhou, 730000, China

3. Department of Earth, Atmospheric, and Planetary Sciences, Purdue University, West Lafayette, Indiana 47907, USA

4. Department of Forestry and Natural Resources, Purdue University, West Lafayette, Indiana 47907, USA

***Authors for correspondence: qbwu@lzb.ac.cn [Q. W.], qzhuang@purdue.edu[Q.Z], apchen1111@gmail.com [A.C.],**

The Cryosphere Discuss., https://doi.org/10.5194/tc-2017-264
Manuscript under review for journal The Cryosphere
Discussion started: 8 December 2017

Abstract

Methane (CH_4) cycle on the Qinghai–Tibetan Plateau (QTP), the world's largest high–elevation permafrost region, is sensitive to climate change and subsequent cryoturbation dynamics. Yet its magnitudes, patterns, and environmental controls are still poorly understood. Here we report results from five continuous year–round CH_4 observation from a typical alpine steppe ecosystem in the QTP permafrost region. Results suggested the QTP permafrost region was a CH_4 sink of -0.86 ± 0.23 g CH_4–C m^{-2} yr^{-1} over 2012 – 2016, a rate higher than that of many other permafrost areas such as Arctic tundra in northern Greenland, Alaska, and western Siberia. Soil temperature and soil water content were dominant factors controlling CH_4 fluxes and their correlations however changed with soil depths due to cryoturbation dynamics. This region was a net CH_4 sink in autumn, but a net source in spring, despite both seasons experienced similar top soil thawing and freeze dynamics. The opposite effect was likely caused by their season–specialized cryoturbation processes, which modified the vertical distribution of soil layers that are highly mixed like a multi–layer hamburger in autumn, but not in spring. Furthermore, the traditional definition of four seasons failed to capture the pattern of annual CH_4 cycle. We developed a new season division method based on soil temperature, bacteria activities, and permafrost active layer thickness, which significantly improved the modelling of annual CH_4 cycle. Collectively, our findings highlight the critical role of fine–scale climate and cryoturbation in driving permafrost CH_4 dynamics, which needs to be better monitored and modelled in Earth system models.

The Cryosphere Discuss., https://doi.org/10.5194/tc-2017-264
Manuscript under review for journal The Cryosphere
Discussion started: 8 December 2017

1. Introduction

Global atmospheric methane concentration [CH_4] resumed to rise since 2007 after remaining stable between the 1990s and 2006 (Rigby et al., 2008; IPCC, 2013; Patra and Kort, 2016). Understanding mechanisms for this recent increase would require improved knowledge on methane (CH_4) sources and sinks for regional and global CH_4 budget (Kirschke et al., 2013; Zona et al., 2016). However, estimates on global CH_4 emissions and consumptions are still highly uncertain (Spahni et al., 2011; Kirschke, 2013). In particular, the bottom–up approach, which estimates CH_4 budget using ground observations and inventory, over–estimated the global CH_4 budget by 6～20 times compared to the atmospherically constrained top–down approach (Zhu et al., 2004; Lau et al., 2015). This discrepancy is partly due to limited monitoring data and partly due to our poor understanding on important factors regulating the production and consumption of CH_4 (Whalen and Reeburgh, 1990; Dengel et al., 2013; Bohn et al., 2015).

The Qinghai–Tibetan Plateau (QTP), the world's largest high–elevation permafrost region of 1.23×10^6 km^{-2} (Wang et al., 2000), is currently experiencing a rapid change in climate which affected cryoturbation processes, profoundly impacting methanotrophy and methanogenesis and consequent net CH_4 fluxes (Mastepanov *et al.*, 2013; Lau et al., 2015). However, due to the scarcity of high temporal–resolution and year–round environment and CH_4 monitoring, we still know little about the size, seasonal pattern, and underlying controls of climate and permafrost cryoturbation and their effects on CH_4 exchanges in the QTP permafrost region (Cao et al., 2008; Wei et al., 2015a; Song et al., 2015;). This knowledge gap would also hamper our capacity in predicting and understanding QTP permafrost CH_4 cycling under current and projected future climates.

Here, we report results from a 5–year continuous *in situ* monitoring of CH_4 dynamics with eddy covariance (EC) technique at the Beilu'he Research Station, a representative site for QTP permafrost heartland covered by alpine steppe vegetation, from January 1st, 2012 to December 31st, 2016. There are three advantages of our data acquisition system. First, the EC system recorded data of CH_4 fluxes and climate, soil properties every half hour. As the QTP permafrost is characterized with rapidly changing climate and soil cryoturbation dynamics even over a short time period like within a day, different aerobic or anaerobic soil environments that favor different types of CH_4 bacteria may also change frequently (Rivkina et al., 2004; Lau et al., 2015). Thus, high–resolution *in situ* monitoring data would enable us to quantify CH_4 exchange patterns from diel to annual time–scales and investigate their major environmental drivers. Second, our field investigation spanned five full calendar years including both plant growing and non–growing seasons. Observations of the plant non–growing season that account for two-thirds of a year were very rare in current literature (Song et al., 2015). Third, the EC system we used overcomes some technical problems caused by the previously often used static chambers, including limited representation of local site heterogeneity and additional heating of the soil surface (Chang et al., 2014; Wei et al., 2015b).

2. Methods

2.1 Site Description

The research site, Beilu'he permafrost research station (34° 09' 006" N, 92° 02' 080" E), is located in the alpine steppe continuous permafrost area of the northern QTP, about 320 kilometers southwest of Golmud (Figure 1). At an elevation of 4765 meters, the air is thin with only 0.6 standard atmospheric pressure. According to *in situ* observations, the site receives solar radiation about 6720 MJ m^{-2}. The non–growing season is long and cold with 225 days per year

and annual air temperature is -18 ℃ on average from 2012 to 2016. Its growing season is short and cool with 140 days per year from 2012 to 2016 and mean annual air temperature is 4.6 ℃. According to the site drilling exploration, the permafrost depth can extend to 50 − 70 m belowground, and the thickness of the active layer (ALT) is about 2.2 − 4.8 m. The soil is composed of Quaternary fine sand or silt (Table 1), overlying on Triassic mudstone or weathered marl. Dominant plant species includes *Carex moorcroftii Falc. ex Boott, Kobresia tibetica Maxim, Androsace tanggulashanensis, Rhodiola tibetica*. Vegetation coverage is approximately 33.5% and average plant height is 15 cm.

2.2 Eddy Covariance observations

We have continuously monitored CH_4, carbon dioxide (CO_2), water (H_2O) and heat flux using a standard eddy covariance system tower 3m above the ground. CH_4 flux was measured with an open-path CH_4 analyzer system (Figure 1: d; LI–7700, LI–COR Inc., Lincoln, NE, USA). The precision is 5 ppb RMS noise at 10 Hz and 2000 ppb. The instrument was placed on site on August 8th, 2011, and then connected to a three–dimensional sonic anemometer (heat and water flux; CSAT3, Campbell Scientific, and Logan, UT, USA; precision is 0.1 ℃; accuracy is within 1% of reading for half–hour) and an open–path infrared gas analyzer (CO_2 flux; LI–7500A, LI–COR Inc., Lincoln, NE, USA; the precision is 0.01μmol m^{-2} s^{-1} and the accuracy is within 1% of reading for half–hour, zero drift per ℃ is ± 0.1 ppm typical) on January 1st, 2012 when the system worked steadily. Monitoring data were recorded and stored 10 Hz using a data logger (LI–7550, LI–COR Inc., Lincoln, NE, USA).

To reduce the LI–7500A surface heating / cooling influence on CO_2 and H_2O molar densities in tough environments. Each year, "summer style" was used in Li–7500A, in which

surface temperature setting is 5℃ during May 1st to September 30th; "winter style" was used from October 1st to the next year April 30th in Li–7500A, in which surface temperature setting is -5℃. Calibrations of CO_2, water vapor, and dew point generator measurements for LI–7500A analyzers were performed regularly by the China Land–Atmosphere Coordinated Observation System (CLAROS). Up–and–down mirrors of LI–COR 7700 were cleaned regularly every 30 days to make sure the signal strength was stronger than 80. All of these instruments were powered by solar–panel and battery.

2.3 Micrometeorological and Soil Measurements

A wide range of meteorological variables was measured by a standard automatic meteorological tower 3 m above the ground and northern 5 m apart from the eddy covariance tower. Rn and albedo were measured with a four–component radiometer (Rn; CNR–1, Kipp and Zonen, the Netherlands). Air temperature (T_{air}), air relative humidity, and atmospheric pressure were measured with a temperature and humidity sensor (HMP45C, Vaisala Inc., Helsinki, Finland) in the meteorological tower. A rain gauge (TE525MM, Texas Electronics Inc., Dallas, TX, USA) was used to measure precipitation process. Wind speed and wind direction were observed using a propeller anemometer placed on the top of the meteorological tower.

Two self–calibrating soil heat flux (SHF) sensors (HFP01) were placed 5 cm and 15 cm below the ground. A group pF–Meter sensor (GEO–Precision, Germany) was embedded in the soil under meteorological tower to measure soil temperature (T_{soil}) at 0 cm, 5 cm, 10 cm, 15 cm, 20 cm, 30 cm, 40 cm, 50 cm, 70 cm, 80 cm, 100 cm, 150 cm, 160 cm, 200 cm depth and soil relative water content (SWC) at 10 cm, 20 cm, 40 cm, 80 cm, and 160cm depth. Both the air temperature, humidity sensors, and pF meter sensors were calibrated in the State Key Laboratory

of Frozen Soil Engineering of the Chinese Academy of Sciences to ensure the measurement accuracy is within ± 0.05 °C and ± 5%, respectively.

All of above environment parameters were synchronously monitored with eddy covariance and the data were recorded every 30 minutes by CR3000 (Data logger, Campbell Data Taker Ltd, Salt Lake City, UT, USA).

In August 2010, one 1 m × 1 m × 2 m pit was dug for soil sample collection and installation of soil environmental sensors, it is 10 m from the eddy covariance tower. Five profile samples were taken from the pit at depths 0 − 20 cm, 20 − 50 cm, 50 − 120 cm, 120 − 160 cm, and 160 − 200 cm. Every depth was repeated for five times, after fully mixed, then stored in soil sample aluminum boxes and carefully sealed to prevent gas exchanges with air. The clod method was used to investigate the field wet bulk density (weight of soil per unit volume; Cate and nelson, 1971). The soil moisture content was calculated gravimetrically by the ratio of the mass of water present to the oven–dry (60 ℃, 24 h) weight of the soil sample. Soil organic carbon (SOC) content of the air–dried soil samples was analyzed using the wet combustion method, Walkley–Black modified acid dichromate digestion, $FeSO_4$ titration, and an automatic titrator. Total Nitrogen (TN) and pH were measured using standard soil test procedures from the Chinese Ecosystem Research Network.

Following Muller's original definition, ALT is the maximum thaw depth in the late autumn using a linear interpolation of Tsoil profiles between two neighboring points above and below the 0 °C isotherm (Muller, 1947). We used records of the soil thawing thickness measured with a self–made geological probe to verify the ALT data semi–monthly. More information about the measurement procedure was previously described (Wu and Zhang, 2010a).

The Cryosphere Discuss., https://doi.org/10.5194/tc-2017-264
Manuscript under review for journal The Cryosphere
Discussion started: 8 December 2017

156 **2.4 Microbial Activity**

157 We sampled 100 gram soils by soil sample drill device (Ø=0.03 m) from 0 − 25 cm depth
158 every 5 days. The sampled soil was fully mixed and divided into two equal parts, storing in
159 sterilized aluminum box placed in liquid nitrogen before sending to the lab for microbe RNA
160 extraction. We then used a real-time PCR method to genetically test r methanotrophic / archaeal
161 methanogens, and the procedure was repeated three times for each sample. By setting the
162 maximum methanotrophic / archaeal methanogens gene expression cyclic number as 1, we
163 calculated the variety coefficient of methanotrophic and archaeal methanogens gene expressions
164 (ΔI and ΔII, respectively; %) with equation (1) :

165 $$\Delta_i = X_I / X_{Max} \quad \ldots \quad (1)$$

166 Δ_i is for the ith methanotrophic/archaeal methanogens gene expression; X_i is the
167 methanotrophic / archaeal methanogen gene expression cyclic number of the ith time; X_{Max} is the
168 maximum methanotrophic / archaeal methanogen gene expression cyclic number of the soil
169 group from 2012 to 2016.

170 **2.5 EC Data Processing and Data Filtering**

171 Data collected from January 1st, 2012 to December 31st, 2016 were used in this study.
172 Before processing, we removed data that were recorded at the time of precipitation events or
173 with LI–7700 signal strength under 85. We first processed the raw data in Eddypro 6.2.0 (LI–
174 COR, Lincoln, NE, USA). We adopted standardized procedures recommended in Lee et al. (2006)
175 to process half–hourly flux raw measurements to ensure their quality:

1) data were processed through statistical analysis in Eddypro 6.2.0 including: spike removal (accepted spikes < 5% and replaced spikes with linear interpolation), amplitude resolution (range of variation: 7.0 σ, number of bins: 100, accepted empty bins: 70%), drop–outs (percentile defining extreme bins: 10, accepted central drop–outs: 10%, accepted extreme drop–outs: 6%), absolute limits (-30 m s^{-1} < U < 30 m s^{-1}, -5 m s^{-1} < W < 5 m s^{-1}, -40 ℃ < Ts < 40 ℃, 200 μmol mol^{-1} < CO_2 < 500 μmol mol^{-1}, 0 μmol mol^{-1} < H_2O < 40 μmol mol^{-1}, 0.17 μmol < CH_4 < 1000 μmol), Skewness and kurtosis (-2.0 < Skewness lower limit < -1.0, 1.0 < Skewness up limit < 2.0; 1.0 < Kurtosis lower limit < 2.0, 5.0 < Kurtosis upper limit < 8.0), discontinuities (hard–flag threshold: U = 4.0, W = 2.0, T_S = 4.0, CO_2 = 40, CH_4 = 40, and H_2O = 3.26; soft–flag threshold: U = 2.7, W = 1.3, T_S = 2.7, CO_2 = 27, CH_4 = 30, and H_2O = 2.2), angle of attack (minimum angle of attack = -30, maximum angle attack = 30, accepted amount of outliers = 10%), steadiness of horizontal wind (accepted wind relative instationarity = 0.5) (Vickers and Mahrt, 1997; Mauder et al., 2013).

2) The data were then corrected using atmosphere physical calculation expressed by: axis rotations of tilt correction (double rotation), time lags compensation (covariance maximization), and compensating density fluctuations of Webb–Pearman–Leuning (WPL) terms. When CO_2 and H_2O molar densities are measured with the LI–COR 7500 / LI–COR 7500A in cold environments (low temperatures below -10 ℃), a correction should be applied to account for the additional instrument–related sensible heat flux, due to instrument surface heating / cooling. Thus, we implemented the correction according of Burba et al. (2008), which involves calculating a corrected sensible heat flux (H') by adding estimated sensible heat fluxes from key instrument surface elements, including the bottom window (H_{bot}), top window (H_{top}), and spar (H_{spar})—to the ambient sensible heat flux (H):

The Cryosphere Discuss., https://doi.org/10.5194/tc-2017-264
Manuscript under review for journal The Cryosphere
Discussion started: 8 December 2017

$$H' = H + H_{bot} + H_{top} + 0.15 \times H_{spar} \quad \ldots \quad (2)$$

3) Quality assurance (QA) / quality control (AC) were ensured through spectral analysis and corrections analysis in Eddypro 6.2.0: spectra and co–spectra calculation used power–of–two samples to speed up the Fast Fourier Transform (FFT) algorithm. Spectra and co–spectra QA / AC by filter (co)spectra were made according to Vickers and Mahrt (1997) test results, and micrometeorological quality test results (Mauder and Foken, 2004). Low–frequency range spectral correction was done considering high–pass filtering effects. High–frequency range spectral correction was done considering low–pass filtering effects (Moncrieff et al., 2004).

4) We chose values "0","1","2" to flag the processed flux data into three quality classes in Eddypro 6.2.0. The combined flag attains the value "0" for best quality fluxes, "1" for fluxes suitable for general analysis such as annual budgets and "2" for fluxes that should be discarded from the results dataset. For our dataset, approximately 67% of the data fell into Class 0, 12% in Class 1, and 21% in Class 2.

5) Our analysis indicated that, under average meteorological conditions, 80% of the flux came from area within 175 m of the eddy covariance tower.

In addition, we also adopted the method in Burba et al. (2008) to adjust the half–hour flux data to avoid apparent measuring errors. In doing this, we rejected half–hour flux data that fall into one of the following situations: (1) incomplete half–hour measurements, (2) measurements under rain impacts, (3) nighttime measurements under stable atmospheric conditions (U*, friction velocity, < 0.1 m s^{-1}), and (4) abnormal values detected by a three–dimensional ultrasonic anemometer. This screening resulted in the rejection of about 20.7% of the flux data.

The Cryosphere Discuss., https://doi.org/10.5194/tc-2017-264
Manuscript under review for journal The Cryosphere
Discussion started: 8 December 2017

220 After the above data quality control, there was a 28.7% data gap for CH_4 fluxes over the
221 entire exanimation period. These data gaps were then filled according to the method described in
222 literature (Falge et al., 2001; Papale et al., 2003). We used a linear interpolation to fill the gaps if
223 they were less than 2 hours, a method described in Falge *et al*. (2001) to fill gaps greater than 2
224 hours but less than 1 days, and an artificial neural network approach as described in Papale et al.
225 (2003) and Dengel et al. (2013) to fill gaps greater than 1 day.

226 The quality of the dataset was evaluated using the equation of energy closure:

227 $$EBR = \sum(H + \lambda E) / \sum(R_n - G - S) \quad \ldots. \quad 3$$

228 where the *EBR* is surface energy balance ratio; *H* is heat flux; λE is latent heat; *Rn* is net
229 radiation; *G* is SHF; and *S* is heat storage of vegetation canopy. As vegetation coverage at this
230 research site is sparse, *S* is ignored. From 2012 to 2016, the *EBR* average was larger than 67.5%.

231 We analyzed two different major sources of CH_4 flux gap–filling uncertainty: the first
232 kind of uncertainty came from U* threshold estimate. Following Burba et al. (2008), we
233 excluded the probably false low CH_4 flux at low U*, but how to decide the U* threshold still
234 remained highly uncertain. For instance, when choosing a lower U* threshold, the associated
235 lower flux would contribute to the gap filling and the annual gross (Loescher, et al., 2006). The
236 variance from 5% to 95% of bootstrap provided an average of the uncertainties caused by the U*
237 filter out. The second uncertainty source was due to insufficient power supply. In this research,
238 all instrument power was supplied by solar. Long-time rainy, cloudy, and snow weather, would
239 cause the instrument to stop working by insufficient power supply. When we used the method to
240 fill the gap mentioned above, it would cause the CH_4 deviated from the true value. To our

241 knowledge, the CH_4 flux data were with large uncertainty under rainy conditions.

242 **2.7 Statistical Analyses**

243 We performed correlation, principal component analyses (PCA) and linear regression
244 analyses in IBM SPSS (IBM SPSS Statistics 24; IBM, Armonk NY, USA). Specifically, we used
245 bivariate correlation to examine pairwise relationships between environmental factors and CH_4
246 fluxes, PCA and linear regressions to explore the sensitivity of CH_4 fluxes to simultaneous
247 environmental fluctuations in wind speed, Tair, air relative humidity, Rn, vapor pressure deficit
248 (VPD), albedo, SHF, SWC, and Tsoil. Before performing PCA and linear regressions, the entire
249 dataset was examined for outliers (Cook's Distance, < 0.002), homogeneity of variance (Levene
250 test, $p < 0.05$), normality (Kolmogorov–Smirnov test, smooth line for histogram of Studentized
251 residuals), collinearity (variance inflation factor, $0 < VIF < 10$), potential interactions (*t*–test, $p <$
252 0.05), and independence of observations (*t*–test, $p < 0.05$).

253 We performed structural equation modeling (SEM) to evaluate the effects of
254 environmental variables on CH_4 fluxes for different seasons. SEM is a widely-used multivariate
255 statistical tool that incorporates factor analysis, path analysis, and maximum likelihood analysis.
256 This method uses *priori* knowledge on the relationships between focus variables to verify the
257 validity of hypotheses. Here we performed SEM analyses with AMOS 21.0 (Amos Development
258 Corporation, Chicago, IL, USA). All data are presented as mean values with standard deviations.

259 **3. Results**

260 **3.1 Meteorological Conditions**

261 Environmental factors were observed according to meteorological records from the
262 Beilu'he Permafrost Weather Station from 2012 to 2016. Mean annual Tair was -4.5 ℃ (Figure

263 2), with minimum and maximum mean diel temperatures of -21.6 ℃ (12th January, 2012) and
264 13.8 ℃ (28th July, 2015), respectively. Average net radiation (Rn) was 82.8 Wm^{-2}, while the
265 maximum was in August (136.2 Wm^{-2}; Figure 3). The average VPD was about 0.3, while the
266 maximum was 0.98 and the minimum was 0.02 (Figure 4). Mean annual precipitation was 335.4
267 mm (Figure 5), which was primarily based on rain and snowfall (only occupied 7%). It is very
268 different from the high-latitude permafrost area. From 2012 to 2016, the maximum precipitation
269 was 2013 (488.3 mm), and the minimum was the 2015 (310.0 mm). The main contribution of
270 precipitation was in summer, about 92%. During winter, the precipitation was rare and the mean
271 value was about 6.7 mm, and even decreased from 14.2 mm in 2012 to 2.1 mm in 2016. Spring
272 was another important rainfall period besides summer, in which mean precipitation was about
273 37.5 mm, 8～17% of the total.

274 Figure 6 and Figure 7 showed the SWC and Tsoil varieties of soil layers from 2012 to
275 2016, respectively. Mean SWC of depths 10 cm, 20 cm, 40 cm, 80 cm, and 160 cm were 14%,
276 9%, 8%, 14% and 19%, respectively. Tsoil of depths 0 cm, 5 cm, 10 cm, 20 cm, 30 cm, 40 cm,
277 50 cm 70 cm and 80 cm were along with the Tair changes, but at depths 100 cm, 150 cm, 160 cm
278 and 200 cm were not. The Tsoil of depth 200 cm had a remarkable difference from Tsoil of
279 other layers. The reason could be that some peats exist in this layer and during winter the peat
280 layer were not completely frozen. Figure 8 showed that SHF half-hour and diel scale varieties of
281 5 cm and 15 cm depth. Annual mean value of SHF at 5 cm and 15 cm depth is 7.6 Wm^{-2} and 6.8
282 Wm^{-2}, respectively.

283 The Beilu'he has a windy environment (Figure 9). Its annual average speed was 4.4 m s^{-1}
284 from 2012 to 2016, while its maximum and minimum wind speeds were 14.6 m s^{-1} on 14th

February, 2016 and 1.3 m s^{-1} on 1st November, 2013, respectively. Its winter, spring, and autumn average wind speed were 5.4 m s^{-1}, 4.3 m s^{-1}, and 3.7 m s^{-1}, respectively, while the principal direction of the strongest winds were from the southwest. Late autumn, winter, and early spring drought increased risks of dust blowing days of 122 within a year on average. Its summer average wind speed was about 3.30 m s^{-1}, with the southeast wind dominated.

Figure 10 illustrates the processes of soil freezing and thawing observed from January 2012 to December 2016. The duration of the active layer in the thawing state at 40 cm depth ranged from 174 to 188 days with an average variation of up to 14 days. The average ALT is 4.4 m from 2012 to 2016.

3.2 New classification system of the four seasons

Based on microbial activities (Figure 11), ALT variety coefficients (ALT variety coefficient = $(ALT_{i+1} - ALT_i) / ALT_{Max}$, where ALT_{Max} is the maximum of ALT per year), and Tsoil, we re–defined the four seasons of spring_, summer_, autumn_, and winter_. Below we describe the start date of each season. The end date of a season is the day immediately before the start of the next season. Spring_ starts at the first day of two consecutive observation periods fulfilling both (1) $(\Delta II + \Delta I) / 2 \geqslant 15\%$, and (2) the ALT variety coefficient $\geqslant 0.05$. Summer_ starts on the first day of two consecutive observation periods when (1) $(\Delta II + \Delta I) / 2 \geqslant 45\%$, (2) ALT variety coefficient $\geqslant 0.35$, and (3) five successive days with Tsoil at 40 cm soil depth $\geqslant$ 0 ℃. Autumn_ starts on the first day of two consecutive observation periods when (1) $(\Delta II + \Delta I) / 2 \geqslant 55\%$, (2) the ALT variety coefficient $\geqslant 0.60$, and (3) five successive days the Tsoil of 10 cm $<$ 5 ℃. Winter_ starts on the first day of two consecutive observation periods that (1) $(\Delta II + \Delta I) / 2 < 15\%$ and the ALT variety coefficient < 0.05.

The Cryosphere Discuss., https://doi.org/10.5194/tc-2017-264
Manuscript under review for journal The Cryosphere
Discussion started: 8 December 2017

307 To test the robust of our new division method of seasons in our methane cycle analysis,
308 we compared empirical CH_4 flux estimates using different season definitions (Table 2). In
309 addition to our new method that was based on top soil microbe activity, Tsoil of 0 – 40 cm, and
310 permafrost active layer variability (hereafter refer to as SMT), we also used three conventional
311 methods–one on vegetation cover and temperature change (VCT), one on Julian months (JMC),
312 and the other one on vegetation phenology change (VPC). Specifically, the VCT method splits a
313 year into plant growing season and non–growing season; the JMC method assumes May to
314 October as plant growing season, and November to the following April as non–growing season;
315 and the VPC method defines plant growing season as the period between when all dominant
316 grass species (*Carex Moorcroft Falc. ex Boott*, *Kobresia tibetica Maxim*, *Androsace*
317 *tanggulashanensis*, *Rhodiola tibetica*) germinate and when they all senesce. For each of the four
318 methods, we established empirical maximum likelihood models between all environmental
319 factors and diel CH_4 fluxes over each season and then compared modeled CH_4 fluxes and field
320 observations under those methods of different seasonal definitions (Figure 12). We found that the
321 agreement between modeled and observed CH_4 fluxes using the new SMT method reached R^2 =
322 0.28, almost twice as that of the VPC (R^2 = 0.17) and VCT (R^2 = 0.14) methods, and more than
323 three times that of the JMC method (R^2 = 0.08) (Figure 12). Hence, the comparison suggested
324 that our new method could better model CH_4 fluxes over a year. The use of traditional plant
325 growing season versus non–growing season definitions may also underestimate or overestimate
326 CH_4 sinks or sources, especially when many studies assume CH_4 close to zero during the plant
327 non–growing season. Furthermore, the new SMT method well captures the impact of spring_m
328 and autumn_m permafrost thawing / freezing cycles on CH_4 fluxes, and the different preferable

environments for methanogens and methanotrophic bacteria during the summer_m season, while conventional methods do not.

3.3 Annual, Seasonal and Diel Variabilities of Methane Fluxes

Our results indicated that the Beilu'he site was a CH_4 sink with an annual mean strength of -0.86 ± 0.23 g CH_4–C m^{-2} (95% confidence interval; negative values mean CH_4 sinks, positive values mean CH_4 sources), although the strength of the CH_4 sink varies across different years from -0.57 ± 0.27g CH_4–C m^{-2} yr^{-1} in 2015 to -1.49 ± 0.38g CH_4–C m^{-2} yr^{-1} in 2014 (Figure 5). The amount of gene expression by methanogens and methanotrophs at 0 − 25 cm soils in March and November, for instance, were about 16.8% and 35.6%, respectively, suggesting strong microbial activities even during the cold and dry plant non–growing season (Figure11).

We also observed clearly CH_4 seasonal variations (Figure 13), in both the amount of CH_4 exchanges and their diel cycles (Figure 14). In spring_, the Beilu'he site was a CH_4 source of 0.90 ± 0.37 g CH_4–C m^{-2} yr^{-1} (Figure 13: a), accounting for 53% of annual CH_4 emissions, or 1.81 ± 0.22 mg CH_4–C m^{-2} d^{-1}. For a typical spring_ (Figure 14: a2, b2, c2, d2, and e2), diel CH_4 emission usually started at around 10:00 am ～ 10:30 am, when the thin ice layer on the soil surface started to thaw. It then reached the peak at 12:30 pm ～ 13:30 pm. The emission peak started to weaken at around 15:30 pm ～ 16:00 pm, and reached around zero or even turned into a small sink after 20:00 pm.

In summer_, the Beilu'he site was a CH_4 sink of -0.99 ± 0.18 g CH_4–C m^{-2} yr^{-1} (Figure 13: b), or -13.28 ± 0.38 mg CH_4–C m^{-2} d^{-1}. The diel cycle of CH_4 fluxes in summer_ was characterized with two absorption peaks and one small emission peak (Figure 14: a3, b3, c3, d3, and e3). With Tair increasing after sunrise, soils started to absorb atmospheric CH_4 and this soil

351 uptake process reached its first peak at around 9:30 am ~ 10:30 am. After then the continuously
352 increasing Tair turned to suppress CH_4 uptake and promote CH_4 emissions, likely due to
353 different temperature sensitivities of methanotrophic and methanogenic bacteria. At around
354 15:30pm ~ 16:00 pm when Tair reached the maximum (Figure 2: b), CH_4 emission also reached
355 its peak. The following temperature decrease in the late afternoon again reversed the CH_4 uptake
356 / emission process, and by sunset, we observed another CH_4 sink peak. The rate of CH_4 sink then
357 decreased again through the night with further decreasing temperature.

358 Autumn_ was another season with net CH_4 sink and even had the largest amount of CH_4
359 sink in 2013 (Figure 13: c). The CH_4 sink in autumn_ varied between -0.69 ± 0.19 g CH_4–C m^{-2}
360 (2015) and -1.59 ± 0.33 g CH_4–C m^{-2} (2013), with an average diel rate of -1.19 ± 0.48 g CH_4–C
361 m^{-2} yr^{-1} or -13.31 ± 0.28 mg CH_4–C m^{-2} d^{-1}. The diel dynamics of autumn_ CH_4 fluxes was like a
362 letter "V", with a single sink peak during 13:30 pm ~ 15:30 pm (Figure 14: a4, b4, c4, d4, and
363 e4).

364 In winter_, the net CH_4 flux at the Beilu'he site was an atmospheric source, with an
365 average annual rate of 0.41 ± 0.16 g CH_4–C m^{-2} yr^{-1} or 4.35 ± 0.33 mg CH_4–C m^{-2} d^{-1} (Figure 13:
366 d). It also should be noted that since the investigation started from January 1st, 2012 and ended
367 on December 31st, 2016, the 2011 ~ 2012 and 2016 ~ 2017 winters_ were only about half of
368 the regular length. The diel CH_4 cycle of an average winter_ day was characterized by one single
369 emission peak around 10:30am ~ 17:30 pm (Figure 14: a1, b1, c1, d1, e1 and f1).

370 **3.4 Response to changes in Methane to Environmental Factors**

371 Diel fluxes of CH_4 were highly correlated with many biotic and abiotic environmental
372 factors, either positively or negatively (Table 3). Positive factors include metagenomics of both

373 methanotrophic (r = 0.52, $p < 0.01$) and methanogens (r = 0.49, $p < 0.01$) at 0 − 25 cm soils,
374 ALT (r = 0.43, $p < 0.01$), and wind speed (r = 0.15, $p < 0.01$). Important negative factors include
375 VPD (r = -0.26, $p < 0.01$), SWC at all depths (varied r values between -0.17 and -0.26, $p < 0.01$),
376 Tair (r = -0.11, $p < 0.01$), and air pressure (r = -0.15, $p < 0.01$). The correlation signal between
377 CH_4 fluxes and Tsoil changed with soil depths (varied r values between -0.09 and 0.24, $p < 0.01$).
378 Furthermore, path analysis results showed that Tsoil at 5cm and 10cm were the most important
379 factors, which together contributed about 25% of the relative importance coefficient. Following
380 were SWC at 80 cm (14%) and 20 cm (12%), and Tsoil at 20 cm (8%).

381 Further analyses suggested that dominant control factors of CH_4 fluxes also changed
382 among different seasons. In spring_, Rn was the most important factor with a relative importance
383 coefficient near 60%, followed by SHF at 5 cm (9%) and SWC at 20 cm (6%). Table 4 shows the
384 results of PCA. In spring_, PC1 explained 63% of the CH_4 variations, which was positively
385 correlated with Tair, VPD, Rn, SHF of 15 cm, ALT, ΔI, SWC of 10 – 40 cm, Tsoil of 0 cm,
386 Tsoil of 5 – 20 cm, Tsoil of 30 – 50 cm, and negatively correlated with wind speed. The PC2
387 explained about 23% of CH_4 fluxes variations. PC2 was positively correlated with wind speed,
388 Tair, Rn, SHF of 15cm, but negatively correlated with VPD, ALT, ΔI, SWC 10 – 40 cm, Tsoil of
389 0 cm, Tsoil of 5 – 20 cm, and Tsoil of 30 – 50 cm. The first four principal components explained
390 about 86% of the CH_4 variations.

391 In summer_, the relative importance coefficient of Tsoil at 100 cm and 200 cm was about
392 30.2% and 26.5%, respectively, followed by Tsoil at 70 cm (12.3%) and Tsoil at 0 − 20 cm
393 (11.4%). The first four principal components explained about 88% of the CH_4 variations (Table
394 4). PC1 explained 70% of the CH_4 variations. PC1 was positively correlated with wind speed,
395 Tair, VPD, SHF of 15 cm, ALT, ΔI, SWC of 50 – 160 cm, precipitation, Tsoil of 0 cm, Tsoil of 5

– 40 cm, Tsoil of 50 – 80 cm, and Tsoil of 100 − 200 cm, but negatively correlated with Rn, and SWC of 10 − 40 cm. PC2 was positively correlated with wind speed, Tair, VPD, Rn, SHF of 15cm, SWC of 10 − 40 cm, Tsoil of 0 cm, but negatively correlated with ALT, ΔI, SWC of 50 − 160 cm, precipitation, Tsoil of 5 − 40 cm, Tsoil of 50 − 80 cm, and Tsoil of 100 − 200 cm.

In autumn_, Rn and Tsoil at 5 − 20 cm had the highest relative importance coefficients (18.3%), for Rn and Tsoil is 11.5% and 16.7%, respectively. The first four principal components explained about 86% of the CH_4 variations (Table 4). PC1 explained 69% of the CH_4 variations. PC1 was positively correlated with Tair, VPD, Rn, SHF of 15 cm, ALT, ΔI, SWC of 10 – 40 cm, SWC of 50 – 160 cm, Tsoil of 0 cm, Tsoil of 5 – 40 cm, Tsoil of 50 – 80 cm, and Tsoil of 100 – 200 cm, but negatively correlated with wind speed. PC2 was positively correlated with wind speed, Tair, Rn, SHF of 15 cm, ALT, ΔI, Tsoil of 0 cm, and Tsoil of 5 − 40 cm, but negatively correlated with VPD, SWC of 10 − 40 cm, SWC of 50 − 60 cm, Tsoil of 50 − 80 cm, and Tsoil of 100 − 200 cm.

During winter_, Rn was again the most important factor (34% relative importance coefficient), followed by Tsoil at 0 − 40 cm (27% in total), and SHF of 15 cm (17% in total). The first four principal components explained about 96% of the CH_4 variations (Table 4). PC1 explained 75% of the CH_4 variations. PC1 was positively correlated with wind speed, Tair, VPD, Rn, SHF of 15 cm, ΔI, Tsoil of 0 cm, and Tsoil of 5 − 20 cm. PC2 explained 21% of the CH_4 variations. PC2 was positively correlated with wind speed, Tair, Rn, SHF of 15 cm, and ΔI, but negatively correlated with VPD, Tsoil of 0 cm, and Tsoil of 5 − 20 cm.

4. Discussion

The Cryosphere Discuss., https://doi.org/10.5194/tc-2017-264
Manuscript under review for journal The Cryosphere
Discussion started: 8 December 2017

417 **4.1 New Classification System of the Four Seasons**

418 Here, different from the majority of earlier studies (Treat et al., 2014; Wang et al., 2014;
419 Wei et al., 2015a; Song et al., 2015), we adopted a new classification system of the four seasons
420 based on soil bacteria activities, Tsoil of 0 − 40 cm and ALT, rather than the conventional
421 methods based on Tair and vegetation dynamics (Chen et al., 2011; McGuire et al., 2012).
422 Previous studies indicated that changes in CH_4 fluxes are regulated by soil microbes, and
423 activities of soil microbes are not limited to the warm season (Zhuang et al., 2004; Lau et al.,
424 2015; Yang et al., 2016). For instance, in March and November, we found the amount of gene
425 expression by methanogens and methanotrophs at 0 − 25 cm soils were about 16.8% and 35.6%
426 (Figure 11), respectively, suggesting there are still strong microbial activities during the cold and
427 dry season. Therefore, our new method of defining the four seasons from the top soil's biotic and
428 abiotic features shall better capture the pattern of CH_4 dynamics throughout a year.

429 **4.2 Annual, Season mean and Diel Variability**

430 From 2012 to 2015, the annual mean value was -0.86 ± 0.23 g $CH_4 - C\ m^{-2}$ of the alpine
431 steep ecosystem in Beilu'he. This sink strength is larger than that of previous reports from other
432 sites of the QTP (Cao et al., 2008; Wei et al., 2012; Li et al., 2012; Song et al., 2015; Chang and
433 Shi, 2015) and many high − latitude Arctic tundra ecosystems like northeast Greenland
434 (Jørgensen et al., 2015), western Siberia (Liebner et al., 2011), and Alaska (Whalen et al., 1992;
435 Zhuang et al., 2004; Whalen, 2005). Different hydrothermal conditions, which greatly influence
436 CH_4 cycling in permafrost regions (Spahni et al., 2011; Kirschke et al., 2013), may partly explain
437 the site difference in CH_4 dynamics. For example, compared to the wet and often snow−covered
438 high–latitude Arctic tundra ecosystems, there is no or little snow cover during the cold season in
439 the QTP alpine steppes. Jansson and Taş (2014) pointed out that relatively dry soils could

faciliate the oxidation of CH_4, since the increased number of gaps between soil particles in dry soils enhances the diffusion of oxygen (O_2) and CH_4 molecules and promote aerobic respiration of soil microorganisms (Wang et al., 2014; Song et al., 2015). Meanwhile, unfrozen or capillary water found in cold–season permafrost soils ensures sufficient soil moisture for microbial activities even in relatively drier and cold soils (Panikov and Dedysh, 2000; Rivkina et al., 2004). In addition, many previous studies used static chambers in CH_4 measurements, and may not include plant non–growing season (Wei et al., 2015a; Wang et al., 2014). Static chambers could underestimate CH_4 uptake because of the additional chamber heating-induced CH_4 emissions and frequent measurement gaps from overheating preventive shutdown (Sturtevant et al., 2012).

Cryoturbation processes are of typical characteristics for the QTP permafrost (Wang et al., 2008; Wang et al., 2000; Wu et al., 2010). Our work suggests that cryoturbation dynamics have played a critical role in governing permafrost seasonal and diel CH_4 cycling. For instance, while both spring_ and autumn_ are active seasons for the freeze-thaw dynamics of top soil layers and share many similarities, they have opposite CH_4 processes–soils emit CH_4 during spring_ but consume CH_4 during autumn_ (Figure 13: a and c). We hypothesize that the difference in the cryoturbation process of the two seasons may have played a critical role in determining the direction of CH_4 dynamics. In spring_, the active soil layer thaws from top to bottom (Jin et al., 2000; Cao et al., 2017), and the permafrost table is very shallow (about 10 ～ 45 cm) and is generally water proof (Wu and Zhang, 2008; Song et al., 2015; Lin et al., 2015). The water thawed during the day time would freeze again at night on the soil surface (Shi et al., 2006; Wu and Zhang, 2010b). The thin-ice layer could stop atmospheric gases of CH_4 and O_2 from getting into soils (Gazovic et al., 2010). During autumn_, however, soils are frozen from both top and

bottom and the permafrost table is deep (about 200 ~ 400 cm) (Wu and Zhang, 2010a), which prevents the formation of a layer of thin ice during nighttime surface soil freezing. Instead, the freezing of surface soil reduces soil liquid water content and creates fine gaps that allow CH_4 and O_2 gases into deep soils (Mastepanov et al., 2008; Mastepanov et al., 2013; Zona et al., 2016). Meanwhile, the temperature of deep soils still remains at a relatively high level and methanotrophic bacteria there are still active at this high Tsoil. This could be one important mechanism for autumn_ soil CH_4 consumption.

Furthermore, during the autumn_ thawing–freezing process, the vertical distribution of clay, sandy soils, and soil organic layers was mixed like a multi–layer hamburger structure (Figure 15), rather than forming a gradual change. Similarly, Tsoil, SWC, and soil microbial activities also had this hamburger type of vertical distribution. As a result, layers of frozen and thawed soils were not changing gradually, but appeared like a hamburger structure too. This hamburger–like soil vertical structure trapped high concentration of soil water between the frozen layers, which was therefore highly anaerobic and suitable for CH_4 production. Also because of the hamburger–like structure, biogenic CH_4 between frozen layers could not escape in autumn_, until when the top soil layer was completely frozen in winter_ and created frost cracks. These explain the large burst of CH_4 emission in late autumn_ and early winter_ and may also explain the constant weak CH_4 emission through the winter_ season, although methanogenic bacteria may have stopped functioning in the low temperature of winter_.

4.3 Impacts of Environmental, Permafrost, and Microbial Activities on CH_4 Fluxes

Our results demonstrated the important roles of climate, cryoturbation dynamics, and soil microbe activities in regulating the direction and amount of CH_4 exchanges between the atmosphere and ecosystems in permafrost areas. This was also confirmed by the better

representation of seasonal CH_4 cycles by our new season division method based on soil microbes, temperature, and permafrost dynamics rather than Tair or vegetation phenology. Here we further discuss potential mechanisms of how environmental (including air and soil heat and water), cryoturbation processes, and soil microbes control the production and absorption of CH_4.

First, it is noteworthy that both the strength and direction of correlations between CH_4 fluxes and SWC and Tsoil parameters changed with soil depths, particularly during spring_ and autumn_ when active layer soils shifted between thawing and freezing regularly. The positive and negative CH_4 flux correlations with Tsoil and SWC may suggest that the impacts of Tsoil and SWC on CH_4 fluxes shall be treated as a holistic process rather than separate ones. For instance, in autumn_, the correlation between CH_4 fluxes and Tsoil or SWC was positive at some soil depths, but negative at some other depths, reaching the maximum at the depth of 80 cm. Further *in situ* observations suggested that soil organic matter and soil microbe amount were also at a very high level of this depth, highlighting the regulation of soil abiotic factors on CH_4 cycling may be well influenced by soil biotic activities. In addition, the holistic soil heat–water process could also determine the concentration of soil inorganic ions, particularly during spring_ and autumn_, which were critical factors controlling the amount of soil unfrozen water; and soil unfrozen water in winter may be important for maintaining soil microbial activities (Panikov and Dedysh, 2000; Rivkina et al., 2004).

Tair and precipitation impact CH_4 fluxes indirectly through their influences on Tsoil and SWC (Zhuang et al., 2004; Lecher et al., 2015). Such indirect influences may often be characterized with time–lagged effects (Koven et al., 2011). For instance, post–drought rainfall events in summer_ can first promote soil CH_4 consumption (summer_ of 2014). This is because certain soil moisture is needed for methanogenic bacteria to function (Del et al., 2000; Luo et al.,

509 2012). Yet prolonged rainfall will eventually lead CH_4 fluxes changing from negative (soils
510 consume CH_4) to positive (soils emit CH_4) fluxes. After rainfall events, CH_4 flux gradually
511 turned negative again with the decrease of SWC. As a result of these time–lagged effects, the
512 correlation coefficient between CH_4 fluxes and precipitation often appears very low, although
513 still statistically significant.

514 Second, soil methanogenic and methanotrophic bacteria could co–exist with different
515 optimal niches (e.g., ranges of Tair / Tsoil and SWC; Zhuang et al., 2013; Lau et al., 2015; Wei
516 et al., 2015a). For example, CH_4 diel cycle in summer_ was found to have two strong
517 consumption peaks and one weak emission peak. The timing of these different peaks may well
518 reflect the different environmental requirements for the dominance of methanogens and
519 methanotrophic bacteria. Furthermore, methanogens may have a broader functional temperature
520 range than methanotrophic bacteria (Kolb, 2009; Lau et al., 2015; Yang et al., 2016). This is also
521 evident, for example, by the diel CH_4 cycle in autumn_ when CH_4 consumption was minimal at
522 both lowest and highest Tair.

523 The complex relationships between CH_4 fluxes and environmental factors make it a grand
524 challenge to predict the future of QTP CH_4 budget under changing climate. For instance, it has
525 been generally believed the ALT will increase under projected warming (Wu and Liu, 2004); and
526 the positive correlation between CH_4 fluxes and ALT found here suggests that the QTP
527 permafrost CH_4 sink may thus be weakened. However, the negative correlation between CH_4
528 flux and Tair may lead to a different conclusion. Incorporating our findings and high–resolution
529 data into mechanistic CH_4 models is therefore needed to enhance our capacity in predicting
530 future CH_4 budgets. Earth system models have been introduced to estimate CH_4 dynamics (Curry,
531 2007; Spahni et al., 2011; Bohn et al., 2015). For example, using a terrestrial ecosystem

532 modelling approach, Zhuang et al. (2004) estimated the average QTP permafrost CH_4 sink of -
533 0.08 g C m^{-2} yr^{-1}, much smaller than our field–based CH_4 estimate. Current CH_4 models focus on
534 the regulation of CH_4 processes by temperature and SWC, and usually lack high–resolution data
535 for model parameterization (Bohn et al., 2015). Data interpolation and the use of average values
536 of certain environmental factors are normal practices in most models (Zhuang et al., 2004),
537 which may overlook the impacts of environmental variations on CH_4 dynamics. For example, at
538 Beilu'he, Tair of a typical summer day (e.g., July 6th, 2013) could vary between -6 ℃ and 28 ℃,
539 a difference of 34 ℃. The resulting diel mean temperature, 17 ℃, is beyond the range of
540 methanotrophic bacteria's preferable temperature of 20～30 ℃ (Segers, 1998; Steinkamp et al.,
541 2001; Yang et al., 2016). Therefore, models using diel mean temperature as an input may
542 estimate the site as a net CH_4 sink. However, field observations show a source with a sink only
543 during a short period (8:30am～11:30 am) on July 6th, 2013 because the short–period of the sink
544 was offset by the source over the remaining 21 hours. Furthermore, half–hourly SWC was well
545 related with the waterproof role by permafrost during spring_ and autumn_ (Figure 6: a).
546 However, because of the shortage of high temporal resolution data, half–diel or diel mean SWC
547 data are often used in many previous studies (Zhu et al., 2004; Jiang et al., 2010; Wei et al.,
548 2015b), which could not correctly show the regulation of permafrost soil properties that are
549 critical for CH_4 dynamics. As another example, Tsoil of 0 − 50 cm depth is one of the most
550 important factors related to CH_4 fluxes (Mastepanov et al., 2008). However, many studies used
551 Tair or re–analyzed deep Tsoil instead (Zhu et al., 2004; Bohn et al., 2015; Oh et al., 2016).
552 Because the active layer is not homogeneous but with different thermal conductivities during the
553 cryoturbation process, the use of Tair or deep Tsoil certainly brings in large uncertainties in CH_4
554 modelling. Future research needs to improve mechanistic understanding of CH_4 dynamics and

their biotic and abiotic control factors, and to conduct more high–resolution and long–term field monitoring.

5. Conclusions

Our field data indicate there was a large CH_4 sink in the QTP permafrost area during the recent years. The strength of this CH_4 sink is larger than previous studies in the region and many high–latitude tundra ecosystems. This study highlights the complexity of environmental controls, including soil heat–water processes, permafrost cryoturbation dynamics, and soil microbial activities, on CH_4 cycling. This complexity implies that linear interpolation and extrapolation from site-level studies could introduce large uncertainties in CH_4 flux estimation. Future quantification of CH_4 dynamics in permafrost regions need to account for the effects of complex environmental processes including cryoturbation, and the interaction between heat and water as well as microbial activities. Our findings also highlight the importance of conducting more high–resolution and long–term field monitoring in permafrost regions for better understanding and modelling permafrost CH_4 cycling under a changing climate.

Acknowledgements

We would like to thank Yongzhi Liu, Jing Luo, Ji Chen, Guilong Wu, Wanan Zhu, Zhipeng Xiao, and Chang Liao for their tremendous help in collecting field data over all these years. We also want to pay tribute and gratitude to the late Xiaowen Cui for his contribution to our many field adventures. This study was supported by the National Natural Science Foundation of China (41501083), Opening Research Foundation of Key Laboratory of Land Surface Process and Climate Change in Cold and Arid Regions, Chinese Academy of Sciences (LPCC201307), and Opening Research Foundation of Plateau Atmosphere and Environment Key Laboratory of Sichuan Province (PAEKL − 2014 − C3). A. C. acknowledges the support from a Purdue

University Forestry and Natural Resources research scholarship. The data generated in this study will be freely available on the Asia Flux regional network server (https://db.cger.nies.go.jp/asiafluxdb/).

Reference

Bohn T., Melton J., Ito A.: WETCHIMP–WSL: intercomparison of wetland methane emissions models over West Siberia, Biogeosciences, 12, 3321 – 3349, 2015.

Burba, G. G., Mcdermitt, D. K., and Grelle, A.: Addressing the influence of instrument surface heat exchange on the measurements of CO_2 flux from open–path gas analyzers. Glob. Change Biol., 14(8), 1854 – 1876, 2008.

Cao G., Xu X., and Long R.: Methane emissions by alpine plant communities in the Qinghai–Tibet Plateau, Biol. Lett., 4, 681 – 684, 2008.

Cao B., Gruber S., Zhang T.: Spatial variability of active layer thickness detected by ground–penetrating radar in the Qilian Mountains, Western China, J. Geophys. Res. Earth Surf., 122, 574 – 591, 2017.

Cate, R. B., and Nelson, L. A.: A simple statistical procedure for partitioning soil test correlation data into two classes, Soil Sci. Soc. Am. J., 35(4), 658 – 660, 1971.

Chang R., Miller C., and Dinardo S.: Methane emissions from Alaska in 2012 from CARVE airborne observations, Proc. Natl. Acad. Sci. U. S. A., 111, 16694 – 16699, 2014.

Chang S. and Shi P.: A review of research on responses of leaf traits to climate change, Chin. J. Plant Ecol., 39, 206 – 216, 2015.

Chen W., Wolf B., and Zheng X.: Annual methane uptake by temperate semiarid steppes as

regulated by stocking rates, aboveground plant biomass and topsoil air permeability. Glob. Change Biol., 17, 2803 – 2816, 2011.

Curry C.: Modeling the soil consumption at atmospheric methane at the global scale. Glob. Biogeochem. Cycles, 21, 1 – 15, 2007.

Dengel S., Zona D., and Sachs T.: Testing the applicability of neural networks as a gap–filling method using CH_4 flux data from high latitude wetlands. Biogeosciences, 10, 8185 – 8200, 2013.

Del G., Parton W., and Mosier A.R.: General CH_4 oxidation model and comparisons of CH_4 oxidation in natural and managed systems, Glob. Biogeochem. Cycles, 14, 999 – 1019, 2000.

Falge, E., Baldocchi, D., and Olson, R.: Gap filling strategies for defensible annual sums of net ecosystem exchange, Agric. For. Meteorol., 107(1), 43 – 69, 2001.

Gažovič M., Kutzbach L., and Schreiber P.: Diurnal dynamics of CH_4 from a boreal peatland during snowmelt. Tellus, B, 62, 133 – 139, 2010.

IPCC, climate change 2013: the physical science basis. Contribution of working group I to the fifth assessment report of the intergovernmental panel on climate change., 2013.

Jansson, J. K. and Tas, N.: The microbial ecology of permafrost, Nat. Rev. Microbiol., 12, 414, 2014.

Jiang C., Yu G., and Fang H.: Short–term effect of increasing nitrogen deposition on CO_2, CH_4 and N_2O fluxes in an alpine meadow on the Qinghai–Tibetan Plateau, China, Atmos. Environ., 44, 2920 – 2926, 2010.

620 Jin H., Li S., and Cheng G.: Permafrost and climatic change in China, Glob. Planet, Change, 26,
621 387 – 404, 2000.

622 Jørgensen, C. J., Johansen, K. M. L., and Westergaard–Nielsen, A.: Net regional methane sink in
623 High Arctic soils of northeast Greenland, Nat. Geosci., 8, 20, 2015.

624 Kirschke, S., Bousquet, P., and Ciais, P.: Three decades of global methane sources and sinks, Nat.
625 Geosci., 6, 813, 2013.

626 Kolb, S.: The quest for atmospheric methane oxidizers in forest soils, Environ. Microbiol.
627 Rep., 1, 336 – 346, 2009

628 Koven C.D., Ringeval B., and Friedlingstein P.: Permafrost carbon–climate feedbacks accelerate
629 global warming, Proc. Natl. Acad. Sci. U. S. A., 108, 14769 – 14774, 2011.

630 Lau M., Stackhouse B.T., and Layton A.C.: An active atmospheric methane sink in high Arctic
631 mineral cryosols. ISME J., 9, 1880 – 1891, 2015.

632 Lecher A.L., Dimova N., and Sparrow K.J.: Methane transport from the active layer to lakes in
633 the Arctic using Toolik Lake, Alaska, as a case study, Proc. Natl. Acad. Sci. U. S. A., 112,
634 3636 – 3640, 2015.

635 Lee, X., Massman, W., and Law, B. (Eds.): Handbook of micrometeorology: a guide for surface
636 flux measurement and analysis (Vol. 29), Springer Science and Business Media, 2006.

637 Li K., Gong Y., and Song W.: Responses of CH_4, CO_2 and N_2O fluxes to increasing nitrogen
638 deposition in alpine grassland of the Tianshan Mountains, Chemosphere, 88, 140 – 143,
639 2012.

640 Liebner S., Zeyer J., and Wagner D.: Methane oxidation associated with submerged brown

641 mosses reduces methane emissions from Siberian polygonal tundra, J. Ecol., 99, 914 – 922,
642 2011.

643 Lin Z., Burn C.R., and Niu F.: The Thermal Regime, including a Reversed Thermal Offset, of
644 Arid Permafrost Sites with Variations in Vegetation Cover Density, Wudaoliang Basin,
645 Qinghai–Tibet Plateau. Permafr. Periglac. Process., 26, 142 – 159, 2015.

646 Loescher, H. W., Law, B. E., and Mahrt, L: Uncertainties in, and interpretation of, carbon flux
647 estimates using the eddy covariance technique. J. Geophys. Res. Atmos., 111(D21), 2006.

648 Luo G.J., Brüggemann N., and Wolf B.: Decadal variability of soil CO_2, NO, N_2O, and CH_4
649 fluxes at the Höglwald Forest, Germany. Biogeosciences, 9, 1741 – 1763, 2012.

650 Mastepanov M., Sigsgaard C., and Dlugokencky E.J.: Large tundra methane burst during onset
651 of freezing. Nature, 456, 628 – 30, 2008.

652 Mastepanov, M., Sigsgaard, C., and Tagesson, T.: Revisiting factors controlling methane
653 emissions from high-Arctic tundra, Biogeosciences, 10(7), 5139, 2013.

654 Mauder, M., Cuntz, M., and Drüe, C.: A strategy for quality and uncertainty assessment of long–
655 term eddy–covariance measurements. Agric. For. Meteorol., 169, 122 – 135, 2013.

656 McGuire A.D., Christensen T.R., and Hayes D.: An assessment of the carbon balance of Arctic
657 tundra: Comparisons among observations, process models, and atmospheric inversions,
658 Biogeosciences, 9, 3185 – 3204, 2012.

659 Moncrieff, J., Clement, R., and Finnigan, J.: Averaging, detrending, and filtering of eddy
660 covariance time series. In Handbook of micrometeorology (pp. 7 – 31), Springer
661 Netherlands, 2004.

662 Muller, S. W. Permafrost or permanently frozen ground and related engineering problems, 1947.

663 Oh Y., Stackhouse B., and Lau M.: A scalable model for methane consumption in arctic mineral
664 soils. Geophys. Res. Lett., 43, 5143 – 5150, 2016.

665 Panikov N.S. and Dedysh S.N.: Cold season CH_4 and CO_2 emission from boreal peat bogs (West
666 Siberia): Winter fluxes and thaw activation dynamics, Glob. Biogeochem. Cycles, 14, 1071
667 – 1080, 2000.

668 Papale, D., Reichstein, M., and Aubinet, M.: Towards a standardized processing of Net
669 Ecosystem Exchange measured with eddy covariance technique: algorithms and uncertainty
670 estimation. Biogeosciences, 3(4), 571 – 583, 2006.

671 Patra P.K. and Kort E.A.:Regional Methane Emission Estimation Based on Observed
672 Atmospheric Concentrations (2002 – 2012), J. Meteor. Soc. Japan. Ser. II, 94, 91 – 113,
673 2016.

674 Rigby M., Prinn R.G., and Fraser P.J.: Renewed growth of atmospheric methane, Geophys. Res.
675 Lett.,35, 2 – 7, 2008.

676 Rivkina E., Laurinavichius K., and McGrath J.: Microbial life in permafrost, Adv. Space Res., 33,
677 1215 – 1221, 2004.

678 Segers R.: Methane production and methane consumptiona–review of processes underlying
679 wetland methane fluxes [Review], Biogeochem., 41, 23 – 51, 1998.

680 Shi P., Sun X., and Xu L.: Net ecosystem CO_2 exchange and controlling factors in a steppe–
681 Kobresia meadow on the Tibetan Plateau. Sci. China Ser. D-Earth Sci., 49, 207 – 218, 2006.

682 Song, W., Wang, H., and Wang, G.: Methane emissions from an alpine wetland on the Tibetan

683 Plateau: Neglected but vital contribution of the non–growing season, J. Geophys. Res.
684 Biogeosci., 120, 1475 – 1490, 2015.

685 Spahni R., Wania R., and Neef L.: Constraining global methane emissions and uptake by
686 ecosystems. Biogeosciences, 8, 1643 – 1665, 2011.

687 Steinkamp R., Butterbach–Bahl K., and Papen H.: Methane oxidation by soils of an N limited
688 and N fertilized spruce forest in the Black Forest, Germany, Soil. Biol. Biochem., 33, 145 –
689 153, 2001.

690 Sturtevant C.S., Oechel W.C., and Zona D.: Soil moisture control over autumn season methane
691 flux, Arctic Coastal Plain of Alaska, Biogeosciences, 9, 1423 – 1440, 2012.

692 Treat C.C., Wollheim W.M., and Varner R.K.: Temperature and peat type control CO_2 and CH_4
693 production in Alaskan permafrost peats, Glob. Chang. Biol. 20, 2674 – 2686, 2014.

694 Vickers, D., and Mahrt, L.: Quality control and flux sampling problems for tower and aircraft
695 data. J. Atmos. Ocean. Technol., 14(3), 512 – 526, 1997.

696 Wang G., Li Y., and Wang Y.: Effects of permafrost thawing on vegetation and soil carbon pool
697 losses on the Qinghai–Tibet Plateau, China, Geoderma, 143, 143 – 152, 2008.

698 Wang S., Jin H., Li S.: Permafrost degradation on the Qinghai–Tibet Plateau and its
699 environmental impacts. Permafr. Periglac. Process., 11, 43 – 53, 2000.

700 Wang Y., Liu H., and Chung H.: Non–growing season soil respiration is controlled by freezing
701 and thawing processes in the summer monsoon‐dominated Tibetan alpine grassland. Glob.
702 Biogeochem. Cycles, 28, 1081 – 1095, 2014.

703 Wei D., Ri X., and Wang Y.: Responses of CO_2, CH_4 and N_2O fluxes to livestock exclosure in an

alpine steppe on the Tibetan Plateau, China. Plant Soil, 359, 45 – 55, 2012.

Wei D., Ri X., and Tarchen T.: Considerable methane uptake by alpine grasslands despite the cold climate: In situ measurements on the central Tibetan Plateau, 2008 – 2013, Glob. Chang Biol., 21, 777 – 788, 2015a.

Wei D., Tarchen T., and Dai D.: Revisiting the role of CH_4 emissions from alpine wetlands on the Tibetan Plateau: Evidence from two in situ measurements at 4758 and 4320 m above sea level, J. Geophys. Res. Biogeosci., 120, 1741 – 1750, 2015b.

Whalen, S. C. and Reeburgh, W. S.: Consumption of atmospheric methane by tundra soils. Nature, 346, 160, 1990.

Whalen S.C.: Biogeochemistry of Methane Exchange between Natural Wetlands and the Atmosphere. Environ. Eng. Sci., 22, 73 – 94, 2005.

Whalen S.C., Reeburgh W.S., and Barber V.A.: Oxidation of methane in boreal forest soils: a comparison of seven measures. Biogeochemistry, 16, 181 – 211, 1992.

Wu Q. and Liu Y.: Ground temperature monitoring and its recent change in Qinghai–Tibet Plateau, Cold Reg. Sci. Technol., 38, 85 – 92, 2004.

Wu Q. and Zhang T.: Recent permafrost warming on the Qinghai–Tibetan Plateau. J. Geophys. Res. Atmos. 113, 1 – 22, 2008.

Wu Q.and Zhang T.: Changes in active layer thickness over the Qinghai–Tibetan Plateau from 1995 to 2007, J. Geophys. Res. Atmos., 115, D09107, 2010a.

Wu Q. Zhang T., and Liu Y.: Permafrost temperatures and thickness on the Qinghai–Tibet Plateau, Glob. Planet. Change, 72, 32 – 38, 2010b.

Yang S., Wen X., and Shi Y.: Hydrocarbon degraders establish at the costs of microbial richness, abundance and keystone taxa after crude oil contamination in permafrost environments. Sci. Rep., 6, 37473, 2016.

Zhu X., Zhuang Q., and Chen M.: Net exchanges of methane and carbon dioxide on the Qinghai–Tibetan Plateau from 1979 to 2100. Environ. Res. Lett., 10, 85007. 2004.

Zhuang Q., Melillo J.M., and Kicklighter D.W.: Methane fluxes between terrestrial ecosystems and the atmosphere at northern high latitudes during the past century: A retrospective analysis with a process–based biogeochemistry model. Glob. Biogeochem. Cycles, 18(3), 2004.

Zhuang Q., Chen M., and Xu K.: Response of global soil consumption of atmospheric methane to changes in atmospheric climate and nitrogen deposition. Glob. Biogeochem. Cycles, 27, 650 – 663, 2013.

Zona D., Gioli B., and Commane R.: Cold season emissions dominate the Arctic tundra methane budget. Proc. Natl. Acad. Sci. U. S. A., 113, 40 – 45, 2016.

Table 1. Soil characteristics at the eddy covariance flux study site

The Cryosphere Discuss., https://doi.org/10.5194/tc-2017-264
Manuscript under review for journal The Cryosphere
Discussion started: 8 December 2017

Soil depth cm	Soil type	Gravel content g kg^{-1}	SOC g kg^{-1}	Microbial Numbers ×10^{4}	pH	DBD g cm^{-3}	SWC %	Total N ×10^{3} mg kg^{-1}
0 − 20	clay	22.3	2.8	3.44	8.7	1.75	18.26	0.87
20 − 50	Silty clay	12.6	1.7	3.82	8.4	1.73	11.52	1.02
50 − 120	silt and fine sand	3.4	1.3	3.67	8.4	1.72	12.57	1.18
120 − 160	silt and fine sand	2.8	26.4	5.44	5.1	1.68	24.69	2.46
160 − 200	silt and fine sand	1.6	13.6	4.39	6.8	1.68	22.45	2.03

745 **Note:** Gravel content diameter ≥ 0.5cm. SOC is soil organic content, DBD is dry bulk density,
746 and SWC is soil water content.
747
748
749
750
751
752
753
754
755

The Cryosphere Discuss., https://doi.org/10.5194/tc-2017-264
Manuscript under review for journal The Cryosphere
Discussion started: 8 December 2017

Table 2. Measurements of four seasons from 2012 to 2016

	Spring_ Period; Total days Days	Summer_ Period; Total days Days	Autumn_ Period; Total days Days	Winter_ Period; Total days Days	Plant growing season Period; Total days Days	Plant non–growing season Period; Total days Days
2012	50 – 142; 93	143 – 229; 87	230 – 323; 94	1 – 49, 324 – 366; 92	139 – 286; 148[a]	1 – 138, 287 – 366; 218[a]
					122 – 305; 184[b]	1 – 121, 306 – 366; 182[b]
					143 – 290; 148[c]	1 – 142, 291 – 366; 218[c]
2013	36 – 137; 102	138 – 224; 87	225 – 334; 110	1 – 35, 335 – 365; 66	139 – 287; 149[a]	1 – 138, 288 – 365; 216[a]
					121 – 304; 184[b]	1 – 120, 305 – 365; 181[b]
					127 – 297; 171[c]	1 – 126, 298 – 365; 194[c]
2014	49 – 127; 79	128 – 228; 101	229 – 309; 81	1 – 48, 310 – 365; 104	137 – 288; 152[a]	1 – 136 , 289 – 365; 213[a]
					121 – 304; 184[b]	1 – 120, 305 – 365; 181[b]
					142 – 294; 153[c]	1 – 141, 295 – 365; 212 [c]
2015	36 – 150; 115	151 – 224; 74	225 – 312; 88	1 – 35, 313 – 365; 88	145 – 288; 144[a]	1 – 144 , 289 – 365; 221[a]
					121 – 304; 184[b]	1 – 120, 305 – 365; 181[b]
					136 – 295; 160[c]	1 – 135, 296 – 365; 205[c]
2016	47 – 161; 115	162 – 225; 64	226 – 299; 74	1 – 46, 300 – 366; 113	141 – 287; 147[a]	1 – 140 , 288 – 366; 219[a]
					122 – 305; 183[b]	1 – 120, 305 – 366; 182[b]
					140 – 296; 157[c]	1 – 139, 297 – 366; 209[c]

The Cryosphere Discuss., https://doi.org/10.5194/tc-2017-264
Manuscript under review for journal The Cryosphere
Discussion started: 8 December 2017

Note: [a], based on vegetation cover and temperature change (VCT) (Lund et al., 2010; Tang and Arnone, 2013; Song et al., 2015); [b], based on Julian months (JMC) (Da et al., 2015); [c], based on vegetation phenology change (VPC). Spring_ , Summer_, Autumn_, Winter_ are based on parameters of microbial activities, ALT variety coefficient and Tsoil (SMT).

The Cryosphere Discuss., https://doi.org/10.5194/tc-2017-264
Manuscript under review for journal The Cryosphere
Discussion started: 8 December 2017

772 **Table 3.** Correlation coefficients between CH_4 fluxes and environment factors on half–hour scales

	CH4 Flux									
Environment	Spring_		Summer_		Fall_		Winter_		2012 − 2016	
Factors	r	n	r	n	r	n	r	n	r	n
T_{air}	0.25**	24144	0.14**	19818	-0.16**	20959	0.32**	22224	-0.11**	87145
Wind Speed	0.31**	24144	-0.04**	19817	-0.20**	20959	0.32**	22224	0.15**	87144
VPD	-0.33**	18624	-0.21**	19263	-0.09**	16737	-0.21	18000	0.26**	69624
Rn	0.55**	24143	0.09**	19807	-0.33**	20913	0.51**	22224	0.09**	87087
Albedo	0.07**	24144	-0.01	19814	-0.08**	20913	0.10**	22224	0.02**	87095
SHF of 5cm	0.46**	24144	-0.08**	19818	-0.23**	20913	0.43**	22224	0.09**	87099
SHF of 15cm	0.36**	24144	-0.15**	19815	-0.23**	20913	0.33**	22224	0.08**	87096
SWC of 10cm	-0.16**	24144	-0.14**	19818	-0.06**	20959	0.00	22224	-0.25**	87145
SWC of 20cm	-0.15**	24144	-0.13**	19816	-0.07**	20959	0.11**	22224	-0.24**	87143
SWC of 40cm	-0.11**	24144	-0.02**	19818	0.07**	20959	0.06**	22224	-0.17**	87145
SWC of 80cm			-0.13**	19818	0.06**	20959				
SWC of 160cm			0.04**	19818	-0.11**	20959				
Precipitation			-0.02	16748	0.01[b]	17888				
ALT	0.73**	23004	0.23**	19823	0.73**	21454			0.43**	64281

ΔI	0.77**	100	0.57**	83	0.46**	89	0.23	93	0.49**	365
ΔII	0.31**	100	0.66**	83	0.78**	89	0.19	93	0.52**	365
T_{soil} of 0 cm	-0.06*	23004	0.13**	19823	0.07**	20366	0.13**	21711	0.11**	84904
T_{soil} of 5 cm	0.15**	24144	0.15**	19808	-0.13**	21454	0.27**	22224	0.24**	87630
T_{soil} of 10 cm	-0.03**	24144	0.12**	19808	0.08**	21454	0.16**	22224	0.13**	87630
T_{soil} of 20 cm	-0.14**	24144	0.08**	19808	0.02**	21454	0.06**	22224	-0.09**	87630
T_{soil} of 30 cm	-0.13**	23004	0.06**	19823	-0.02**	20366	0.07**	21711	-0.08**	84904
T_{soil} of 40 cm	0.14**	24144	0.05**	19808	-0.01[b]	21454	0.06**	22224	0.11**	87630
T_{soil} of 50 cm			0.04**	19823	-0.05**	20366				
T_{soil} of 70 cm			0.07**	19823	-0.05**	20366				
T_{soil} of 80 cm			0.05**	19808	0.04**	21454				
T_{soil} of 100 cm			0.10**	19823	-0.05**	21454				
T_{soil} of 150 cm			0.09**	19823	-0.04**	20366				
T_{soil} of 160 cm			0.10**	19808	0.01**	21454				
T_{soil} of 200 cm			0.02**	19823	-0.02**	20366				

773 **Note:** ** means $p<0.01$, * means $p<0.05$; r values for the relationship between CH_4 flux and environment factors. Tair means air temperature of 3 m
774 above the ground surface. VPD is vapor pressure deficit, NR is net radiation, and SWC is soil water content, ALT is active layer thickness, which
775 fitted through the depth of soil 0 ℃in Surfer 8.0., and the data is removed of meaningless in winter. Tsoil is the temperature of the soil. In spring_ and

The Cryosphere Discuss., https://doi.org/10.5194/tc-2017-264
Manuscript under review for journal The Cryosphere
Discussion started: 8 December 2017

The Cryosphere Discuss., https://doi.org/10.5194/tc-2017-264
Manuscript under review for journal The Cryosphere
Discussion started: 8 December 2017

winter_, precipitation data are too sparse for statistical analysis. ΔI is the soil 0 – 25cm archaeal methanogens gene expression, and Δ II is the soil 0 – 25 cm methanotrophic gene expression. The coefficients (r) between CH_4 flux and ΔI, Δ II are obtained using the synchronous CH_4 fluxes averaged for 5 days.

Table 4. Principal components analysis (PCA) of the environmental factors.

	Spring_				Summer_				autumn_				Winter_			
Component	PC1	PC2	PC3	PC4	PC1	PC2	PC3	PC4	PC1	PC2	PC3	PC4	PC1	PC2	PC3	PC4
wind speed	-0.03	0.51	0.65	-0.46	0.02	0.37	0.38	-0.13	-0.04	0.44	0.59	0.67	0.27	0.45	-0.11	-0.27
Tair	0.38	0.29	-0.05	-0.11	0.42	0.22	-0.03	0.02	0.36	0.21	0.08	-0.06	0.48	0.12	-0.02	0.01
VPD	0.34	-0.27	0.40	0.15	0.17	0.46	-0.22	0.09	0.34	-0.15	0.17	-0.07	0.14	-0.15	0.95	-0.22
Rn	0.16	0.49	0.00	0.76	-0.01	0.07	0.58	0.11	0.12	0.54	-0.43	-0.07	0.26	0.47	-0.01	-0.49
SHF of 15cm	0.24	0.49	-0.30	-0.09	0.25	0.53	-0.09	0.01	0.15	0.59	-0.23	-0.15	0.36	0.37	0.14	0.58
ALT	0.22	-0.40	0.40	0.27	0.32	-0.53	-0.05	0.02	0.29	0.49	0.70	0.25				
ΔI	0.49	-0.22	0.01	-0.08	0.50	-0.16	0.02	-0.16	0.29	0.31	0.24	-0.51	0.52	0.05	0.07	-0.03
SWC of 10 − 20cm													-0.31	0.45	0.22	0.47
SWC of 10 − 40cm	0.33	-0.20	0.50	0.25	-0.16	0.15	-0.16	0.73	0.28	-0.18	-0.41	0.53				
SWC of 50 − 160cm					0.23	-0.20	-0.16	0.55	0.31	-0.17	-0.32	0.41				
Precipitation					0.03	-0.04	0.63	0.35								
Tsoil of 0 cm	0.43	-0.07	-0.20	-0.27	0.43	0.08	0.08	-0.07	0.37	0.07	0.19	-0.16	0.43	-0.35	-0.15	0.09
Tsoil of 5 − 20 cm	0.44	-0.01	-0.17	-0.16									0.45	-0.28	0.00	0.28
Tsoil of 5 − 40 cm					0.46	-0.05	0.04	-0.03	0.38	0.02	0.18	-0.17				
Tsoil of 30 − 50cm	0.40	-0.23	-0.08	-0.04												
Tsoil of 50 − 80cm					0.37	-0.36	0.00	0.01	0.37	-0.11	0.19	-0.14				
Tsoil of 100 − 200cm					0.33	-0.34	0.01	-0.01	0.36	-0.14	0.08	0.00				
Percent of variance	0.63	0.23	0.08	0.04	0.70	0.18	0.07	0.02	0.69	0.17	0.08	0.04	0.75	0.21	0.02	0.01
Cumulative	0.63	0.86	0.94	0.98	0.70	0.88	0.95	0.97	0.69	0.86	0.94	0.98	0.75	0.96	0.98	0.99

Note: PC means principal component. Before PCA, SWC was divided for three parts, 10 – 20 cm, 10 – 40 cm, and 50 – 160 cm according to collinearity test in four seasons. Tsoil was divided for six parts of Tsoil of 0 cm, Tsoil of 5 – 20 cm, Tsoil of 5 – 40 cm, Tsoil of 30 – 50 cm, Tsoil of 50 – 80 cm, and Tsoil of 60 – 200 cm according to collinearity test in different seasons.

The Cryosphere Discuss., https://doi.org/10.5194/tc-2017-264
Manuscript under review for journal The Cryosphere
Discussion started: 8 December 2017

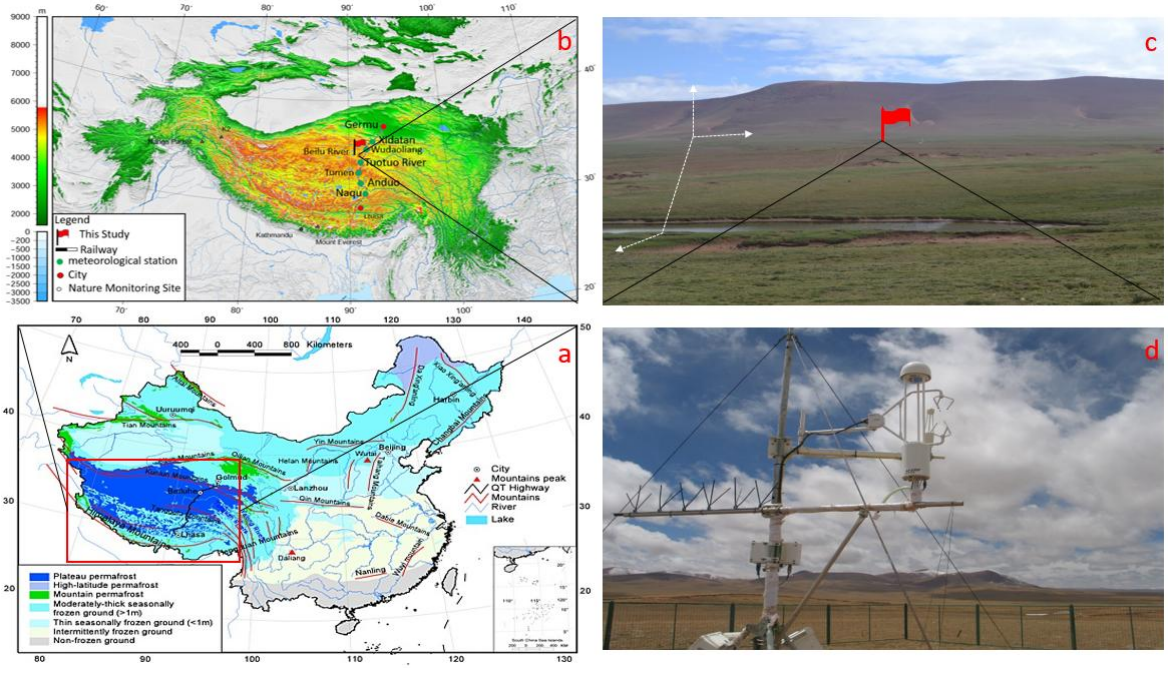

Figure 1. Geographic location of the study site: (a) is a map of China's permafrost distribution, and the red box marks the approximate location of the Qinghai–Tibet Plateau; (b) shows the study site location and meteorological stations along the Qinghai–Tibet railway; (c) is the photo showing the study site's topography and physiognomic. The small red flag in (c) is the eddy covariance tower location; (d) is the close–up shot of the LI–7700 for methane measurement. *Map boundary and location are approximate. Geographic features and the names do not imply any official endorsement or recognition.*

The Cryosphere Discuss., https://doi.org/10.5194/tc-2017-264
Manuscript under review for journal The Cryosphere
Discussion started: 8 December 2017

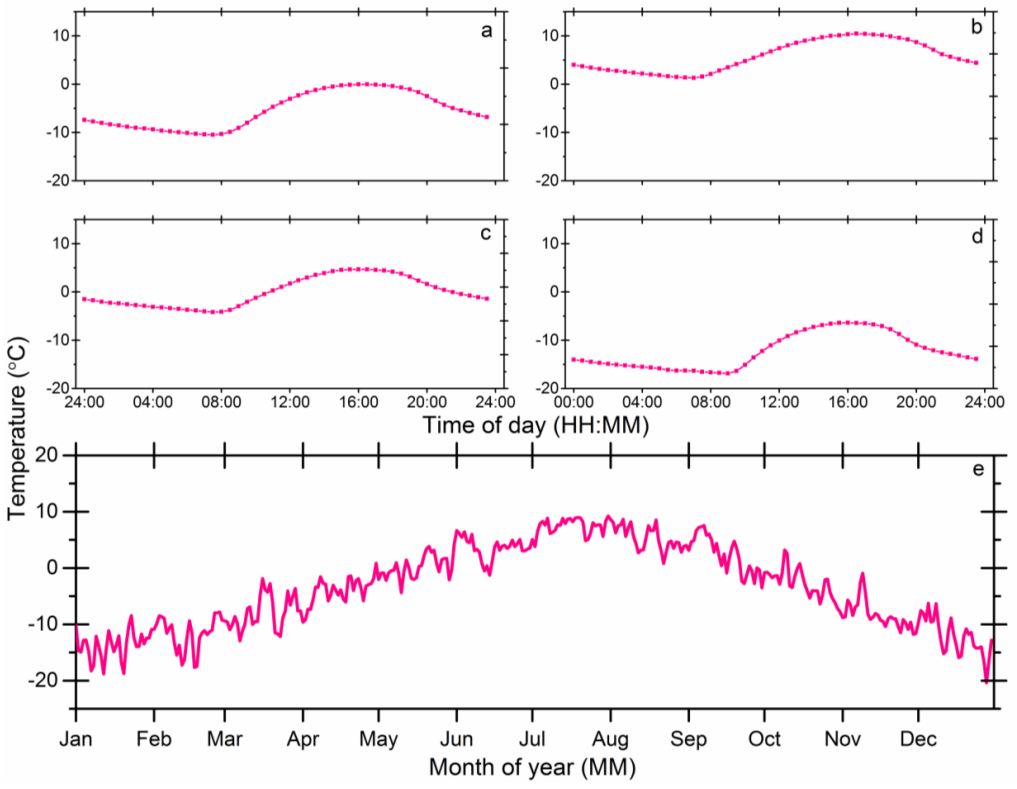

Figure 2. Air temperature (Tair) of 3 meters above the ground surface: (a), (b), (c), and (d) are half–hour scale mean values in spring, summer, autumn, and winter, respectively; (e) shows diel–scale mean values from 2012 to 2016.

The Cryosphere Discuss., https://doi.org/10.5194/tc-2017-264
Manuscript under review for journal The Cryosphere
Discussion started: 8 December 2017

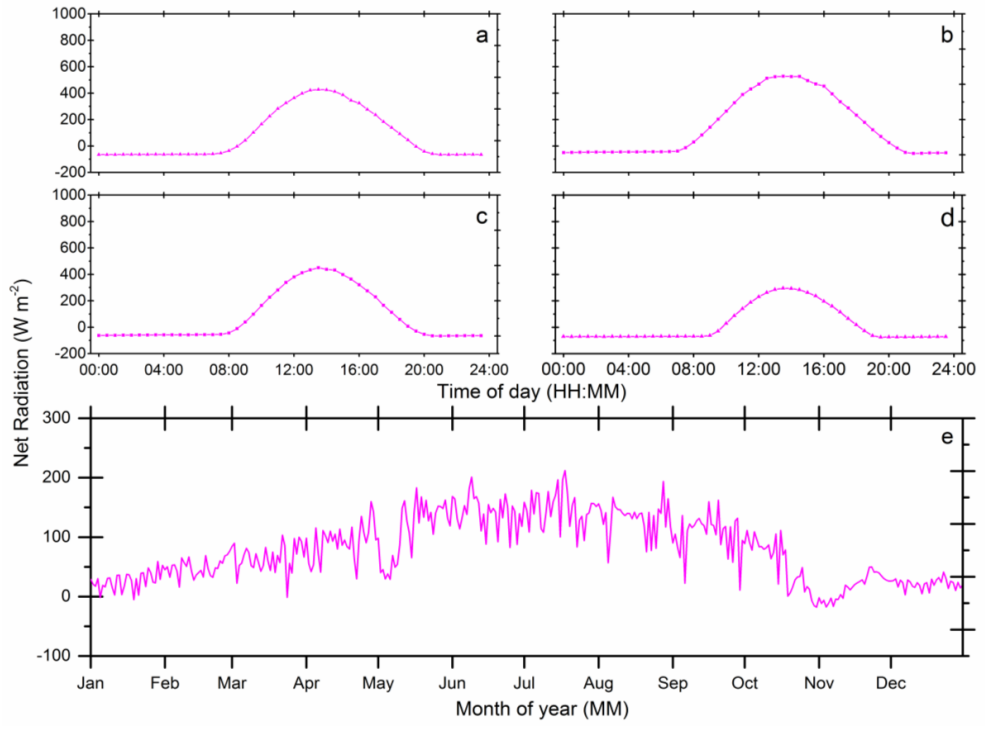

807

808 **Figure 3.** Net radiation (Rn) of 3 meters above the ground surface: (a), (b), (c), and (d) are half–
809 hour scale mean values in spring, summer, autumn, and winter, respectively; (e) shows diel–
810 scale mean values from 2012 to 2016.

811

The Cryosphere Discuss., https://doi.org/10.5194/tc-2017-264
Manuscript under review for journal The Cryosphere
Discussion started: 8 December 2017

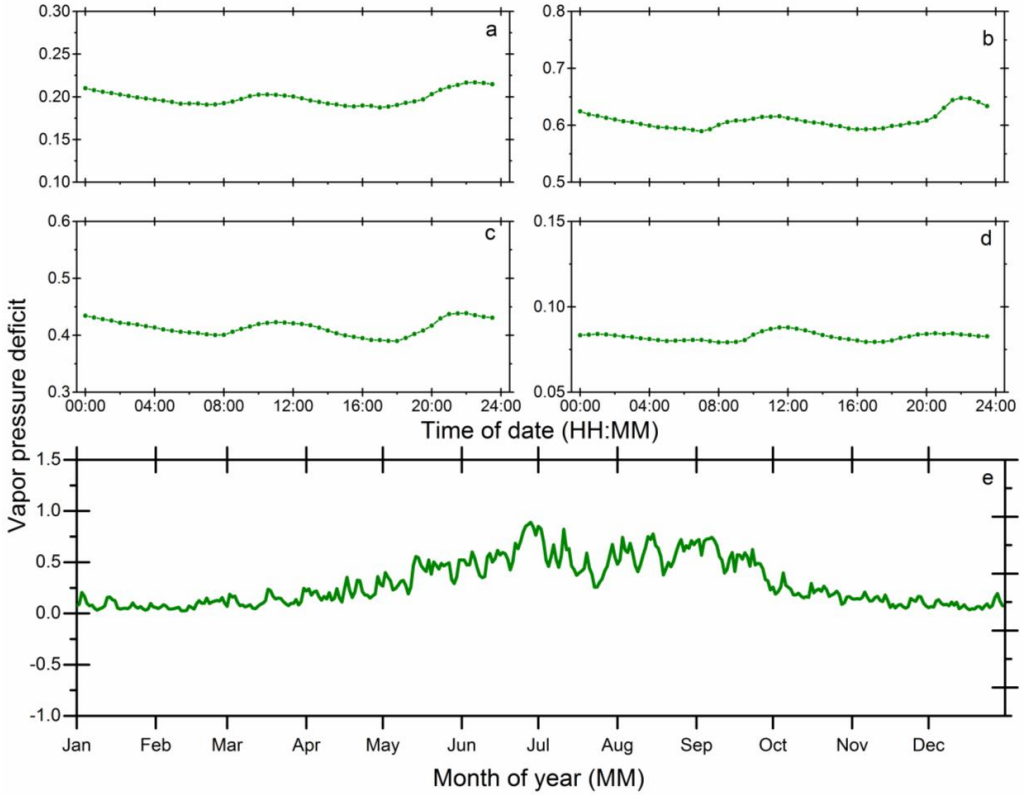

Figure 4. Vapor pressure deficit (VPD) of 3 meters above the ground surface: (a), (b), (c), and (d) are half–hour scale mean values in spring, summer, autumn, and winter, respectively; (e) shows diel–scale mean values from 2012 to 2016.

The Cryosphere Discuss., https://doi.org/10.5194/tc-2017-264
Manuscript under review for journal The Cryosphere
Discussion started: 8 December 2017

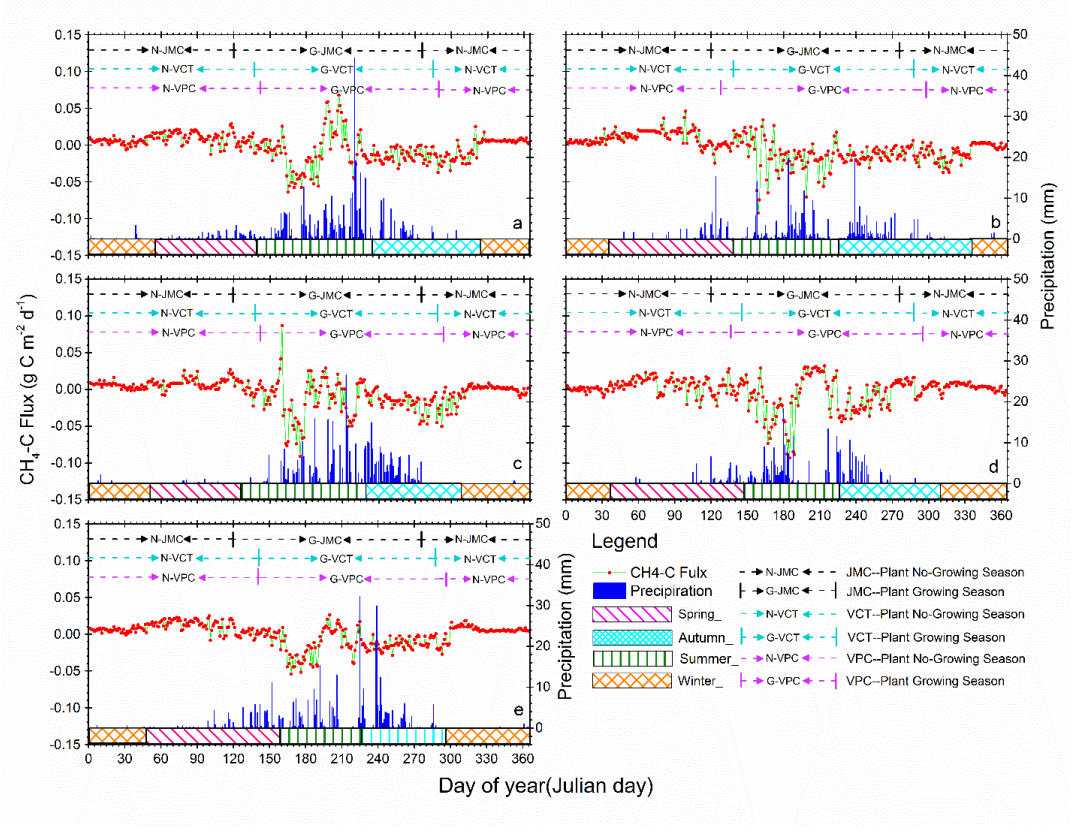

Figure 5. Annual patterns of diel methane (CH_4) flux and precipitation variations from 2012 to 2016. Positive values indicate CH_4 release and negative values indicate CH_4 uptake by ecosystems. Red dots and light green lines are CH_4–C flux variation, and the deep blue histograms show diel precipitation accumulation. Pink, olive, cyan, and orange blocks mean spring, summer, autumn, and winter seasons according to our new method of SMT (see Methods), respectively. Black, cyan, and pink dotted lines with bars separating the plant growing from non–growing seasons stand for seasons by the method JMC, VCT, and VPC, respectively. Details about the methods JMC, VCT, and VPC can be found in Text part 3.2.

The Cryosphere Discuss., https://doi.org/10.5194/tc-2017-264
Manuscript under review for journal The Cryosphere
Discussion started: 8 December 2017

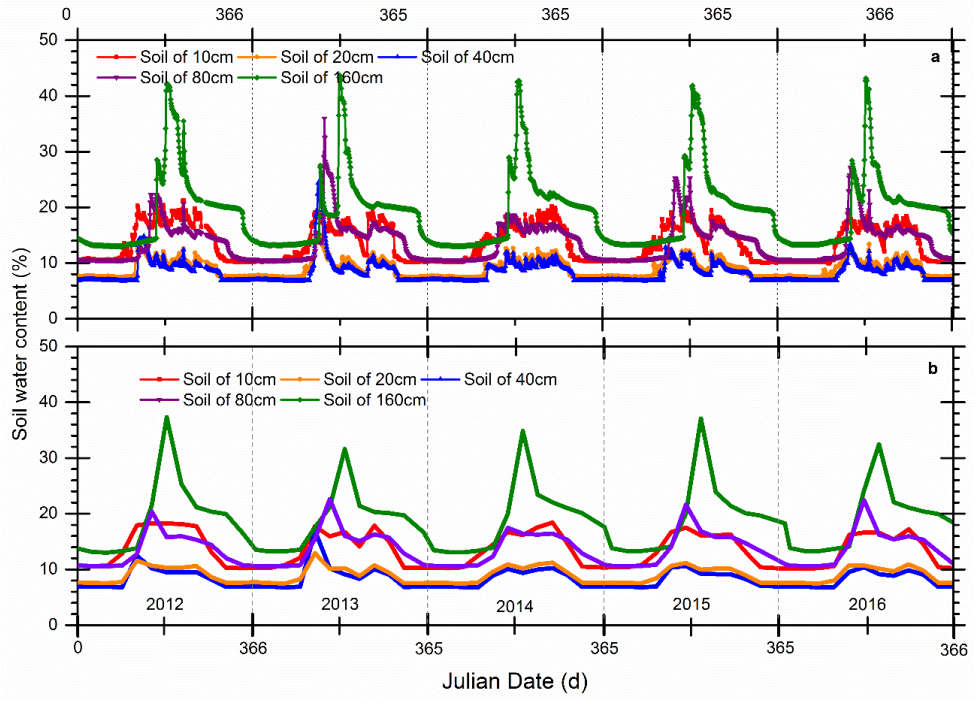

Figure 6. Comparison between soil water content (SWC) of two different time resolutions from 2012 to 2016, (a) is the half–hour scale SWC at soil depths of 10 cm, 20 cm, 40 cm, 80 cm, and 160 cm; and (b) is the 4–hour mean SWC for the same depths.

The Cryosphere Discuss., https://doi.org/10.5194/tc-2017-264
Manuscript under review for journal The Cryosphere
Discussion started: 8 December 2017

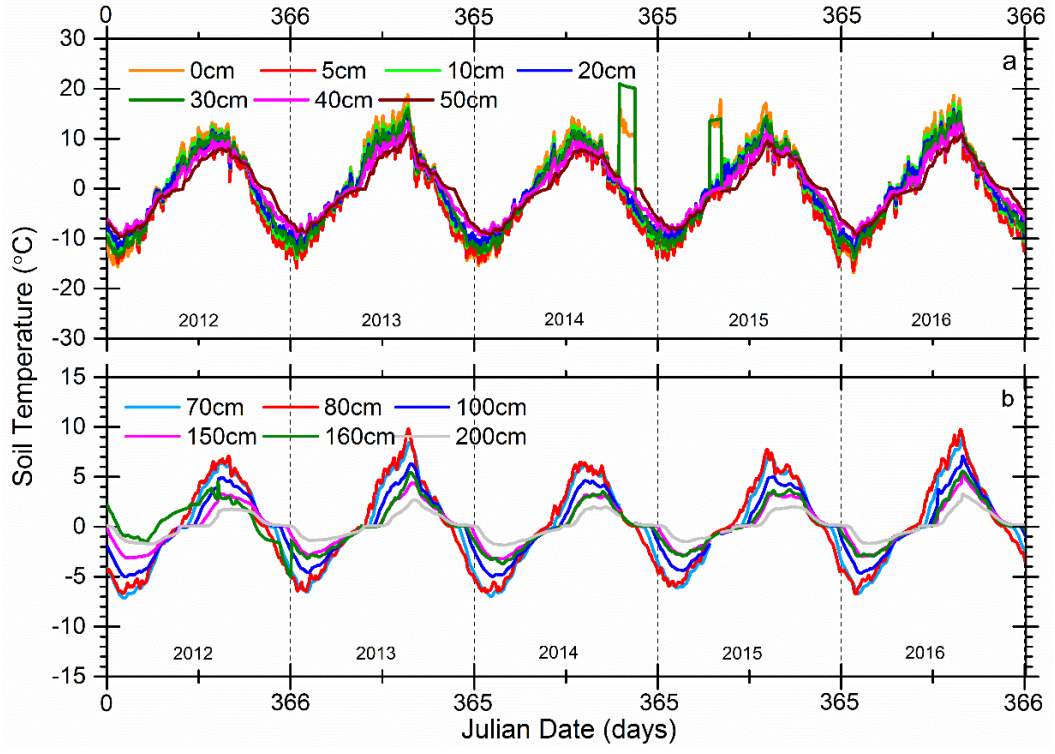

835

836 **Figure 7.** Half–hour scale of 0 − 200 cm soil temperature (Tsoil) variations from 2012 to 2016,

837 (a) is for soil depths of 0 cm, 5 cm, 10 cm, 20 cm, 30 cm, 40 cm, 50 cm, (b) is for soil depth of

838 70 cm, 80 cm, 100 cm, 150 cm, 160 cm, and 200 cm.

The Cryosphere Discuss., https://doi.org/10.5194/tc-2017-264
Manuscript under review for journal The Cryosphere
Discussion started: 8 December 2017

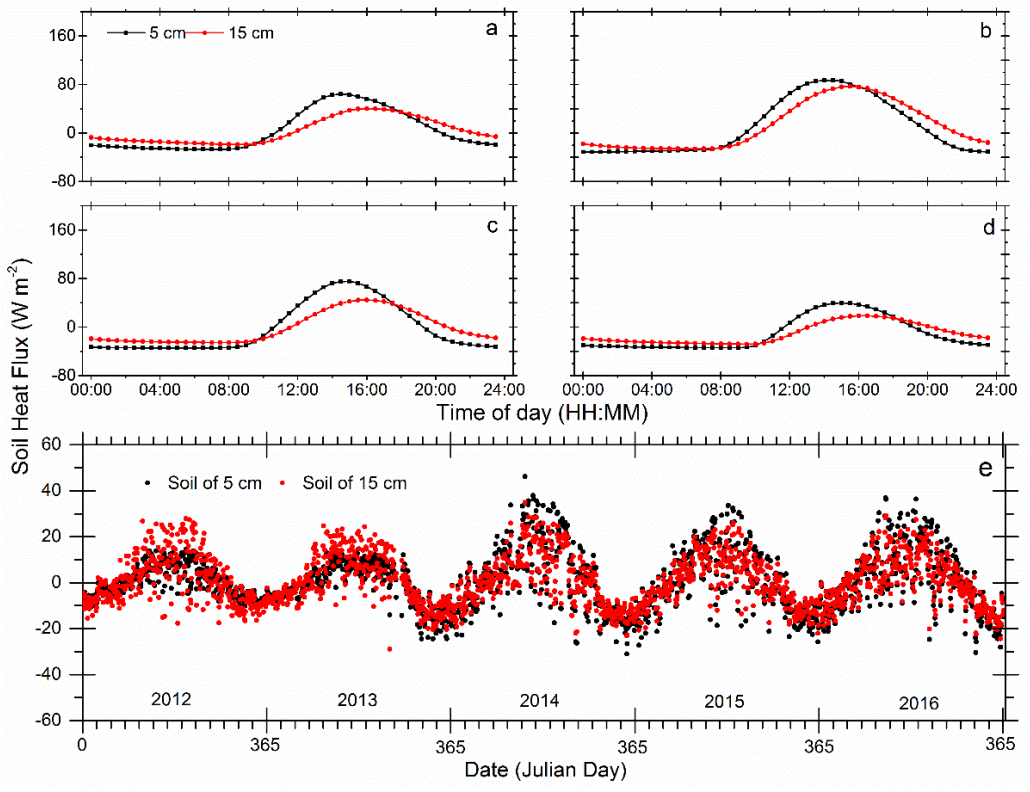

839

840 **Figure 8.** Soil heat flux (SHF) at depth of 5 cm and 15 cm: (a), (b), (c), and (d) are half–hour
841 scale mean values in spring, summer, autumn, and winter, respectively; (e) shows diel–scale
842 mean values from 2012 to 2016.

843

The Cryosphere Discuss., https://doi.org/10.5194/tc-2017-264
Manuscript under review for journal The Cryosphere
Discussion started: 8 December 2017

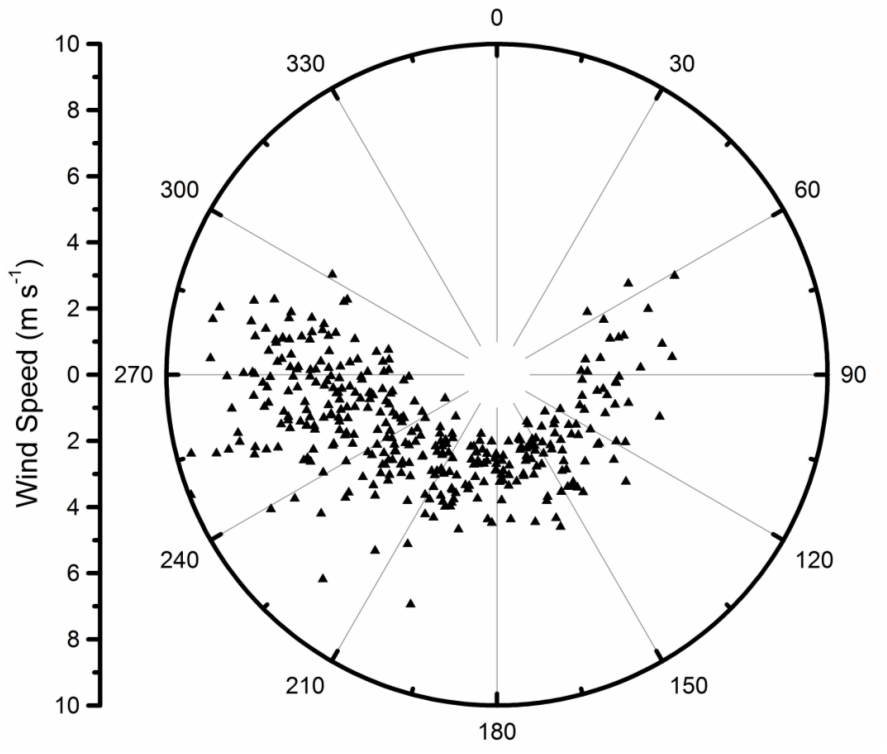

844

845 **Figure 9.** Diel mean of wind speed and direction between 2012 and 2016. All data are presented

846 as mean values with standard deviations (mean ± standard deviation).

847 .

848

849

The Cryosphere Discuss., https://doi.org/10.5194/tc-2017-264
Manuscript under review for journal The Cryosphere
Discussion started: 8 December 2017

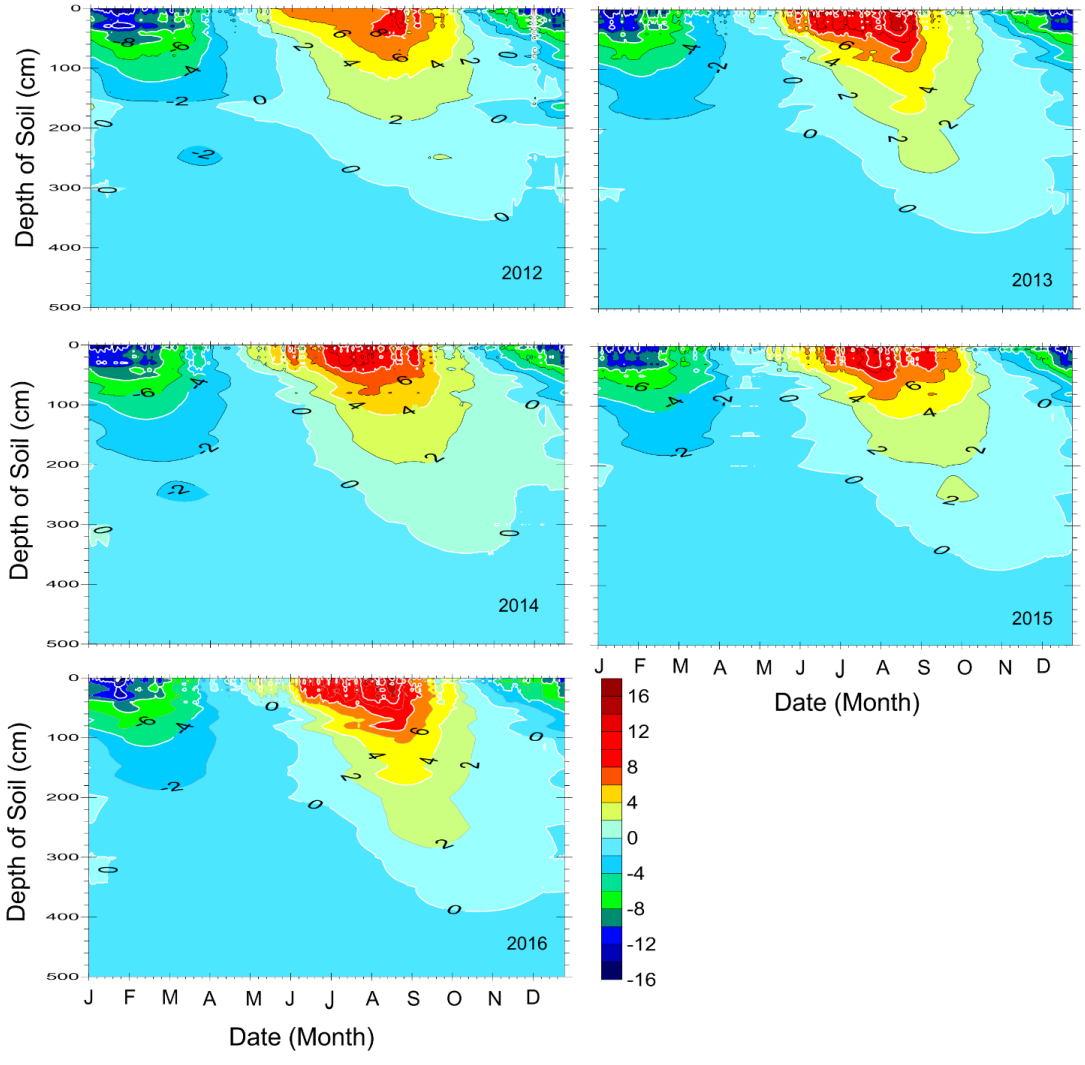

Figure 10. Characteristics of the seasonal freezing and thawing processes of the active layer for years: 2012, 2013, 2014, 2015, and 2016. Different colors represent the soil temperature gradients from -16 ℃ to 20 ℃. The depth of 0 ℃ represent the active layer thickness (ALT).

The Cryosphere Discuss., https://doi.org/10.5194/tc-2017-264
Manuscript under review for journal The Cryosphere
Discussion started: 8 December 2017

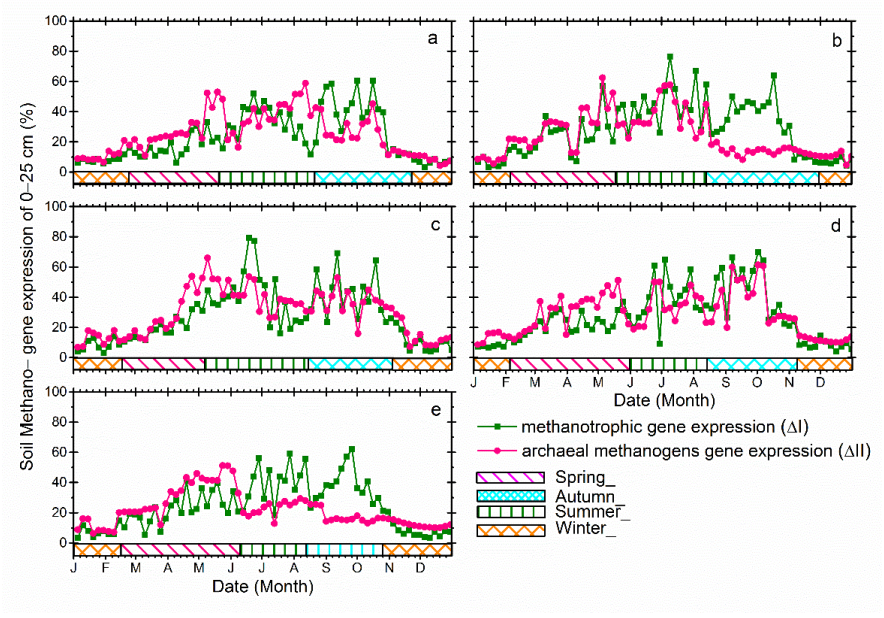

856

857 **Figure 11.** Annual patterns of soil methanogen−gene expression of 0 − 25 cm soil depth for

858 years: (a) 2012, (b) 2013, (c) 2014, (d) 2015, and (e) 2016.

859

860

861

862

The Cryosphere Discuss., https://doi.org/10.5194/tc-2017-264
Manuscript under review for journal The Cryosphere
Discussion started: 8 December 2017

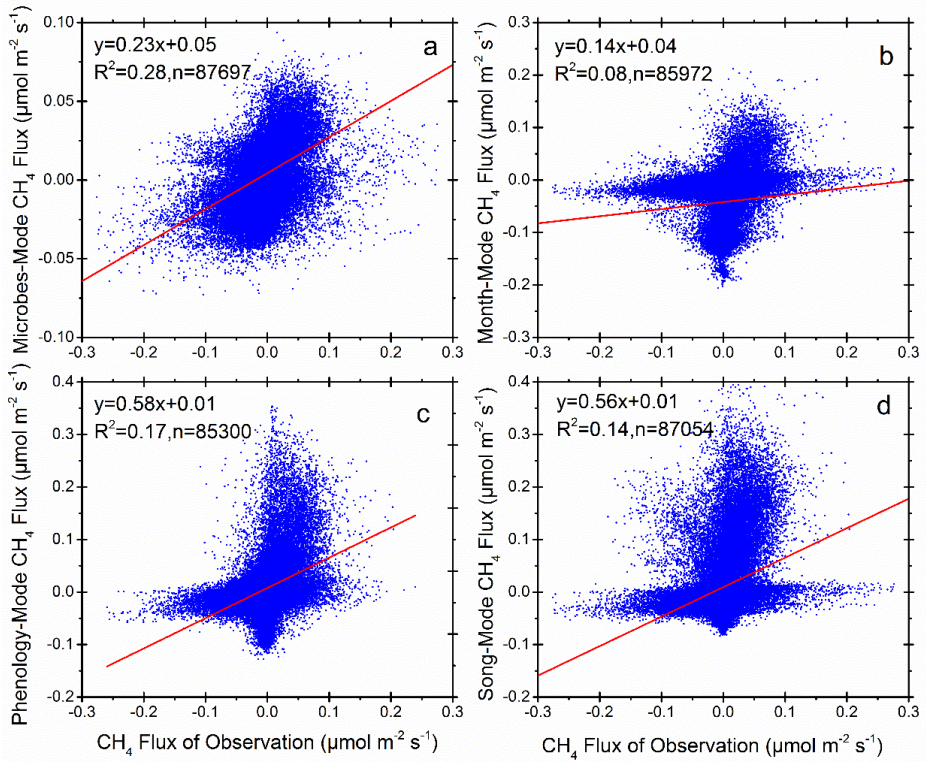

Figure 12. Regression comparison between observation and modeled methane fluxes with four different seasonal definitions and classification models. Panels (a), (b), (c), and (d) are for the SMT, JMC, VCT, and VPC methods, respectively.

The Cryosphere Discuss., https://doi.org/10.5194/tc-2017-264
Manuscript under review for journal The Cryosphere
Discussion started: 8 December 2017

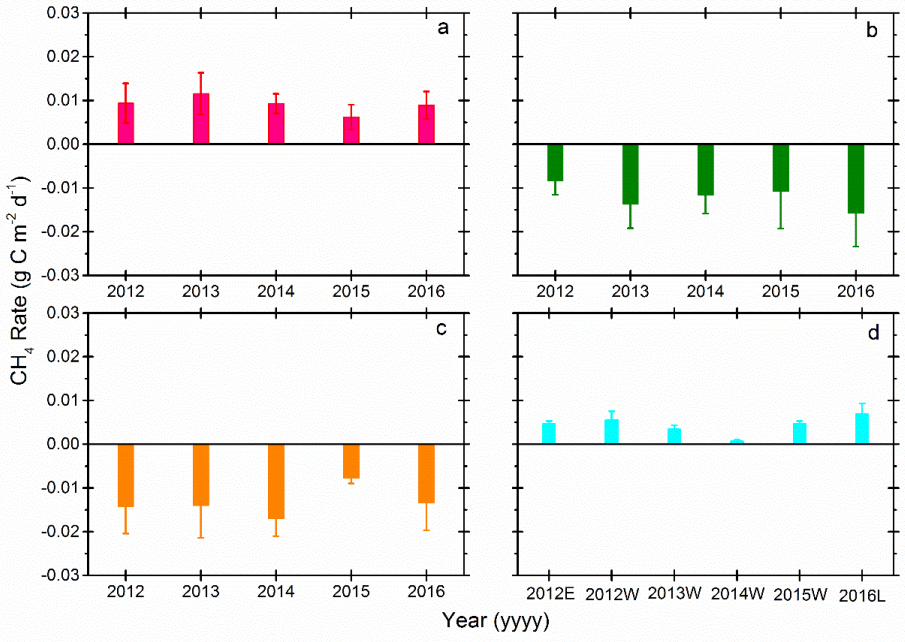

Figure 13. Seasonal CH_4 rate mean value from 2012 to 2016: (a) is spring, (b) is summer, (c) is autumn, and (d) is winter. In the (c), 2012E is started from January 1st, 2012 and ended on February 17th, 2012; 2012W is started from 19th November, 2012 to 4th February, 2013; 2013W is started from 1st December, 2013 to 17th February, 2014; 2014W is started from 6th November, 2014 to 4th February, 2015; 2015W is started from 9th November, 2015 to 15th February, 2016; 2016L is started from October 26th, 2016 and ended on December 31st, 2016. All data are presented as mean values with standard deviations (mean ± standard deviation).

The Cryosphere Discuss., https://doi.org/10.5194/tc-2017-264
Manuscript under review for journal The Cryosphere
Discussion started: 8 December 2017

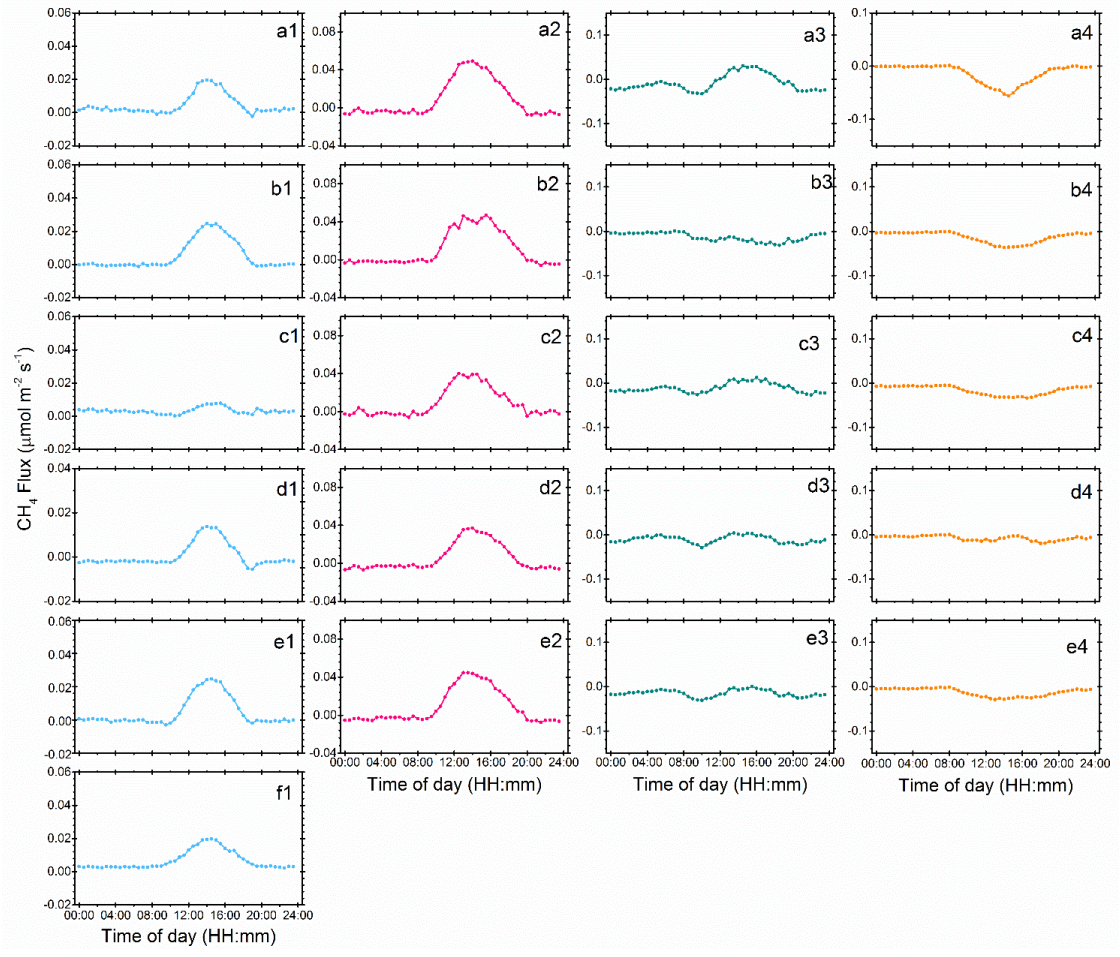

881

882 **Figure 14.** Diel CH_4 fluxes from 2012 to 2016 for different seasons. Pink, green, orange and
883 blue, represent spring, summer, autumn, and winter, respectively; (a1), (a2), (a3), and (a4) are for
884 2012; (b1), (b2), (b3), and (b4) are for 2013; (c1), (c2), (c3) and (c4) are for 2014; (d1), (d2),
885 (d3), and (d4) are for 2015; (e1), (e2), (e3), (e4) and (f1) are for 2016.

886

887

The Cryosphere Discuss., https://doi.org/10.5194/tc-2017-264
Manuscript under review for journal The Cryosphere
Discussion started: 8 December 2017

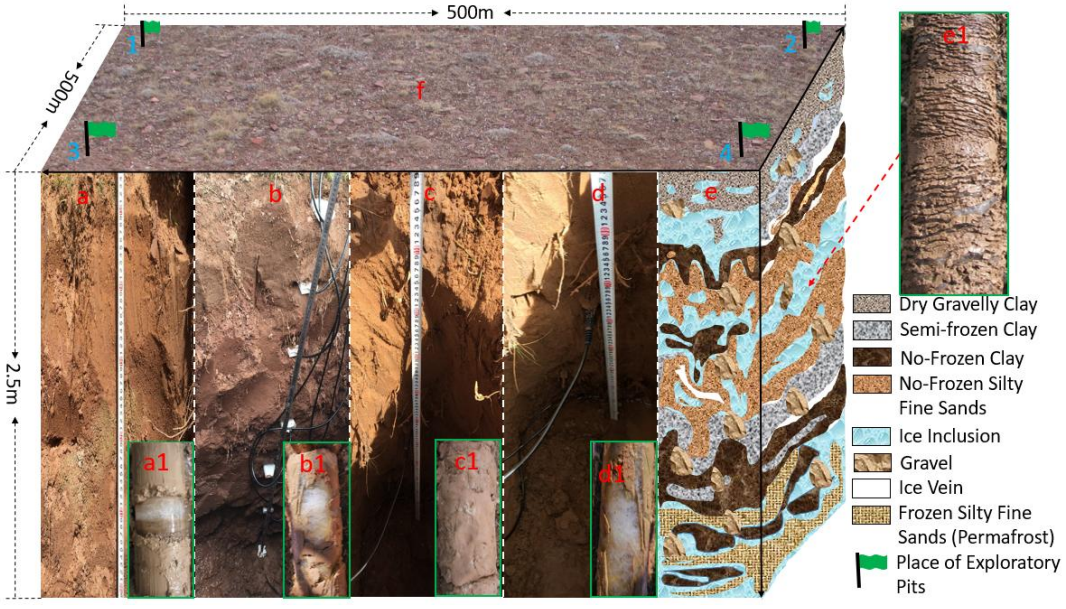

Figure 15. Location of exploratory pits and drillings in this study in autumn: (f) is photo of a typical ground surface (October 16th, 2014). Green flags represent the location for soil survey by test pitting and drilling. (a), (b), (c), and (d) are test pitting sections for active layer 0 − 250 cm depths soil water content and temperature measured in eddy covariance North (1), South (2), East (3), and West (4) corners, respectively. (a1), (b1), (c1), and (d1) are drilling cores, with clear ice (white) in (a1), (b1), and (d1), but not in (c1); (e) provides an illustration that combines results from drillings, test pitting and multi–channel ground–penetrating radar (Malå Geoscience, Sweden) for active layer variations in permafrost area during the autumn season; and (e1) is a core sample of the same drilling (October 16th, 2014).